Title

Dlg5 Regulates Dendritic Spine Formation and Synaptogenesis by Controlling Subcellular N-Cadherin Localization

Journal

Journal of Neuroscience, 34(38)

ISSN

0270-6474

Authors

Wang, Shih-Hsiu J
Celic, Ivana
Choi, Se-Young
et al.

Publication Date

2014-09-17

DOI

10.1523/jneurosci.1280-14.2014

Peer reviewed

Development/Plasticity/Repair

Dlg5 Regulates Dendritic Spine Formation and Synaptogenesis by Controlling Subcellular *N*-Cadherin Localization

Shih-Hsiu J. Wang,[1,2]* Ivana Celic,[1,2]* Se-Young Choi,[1,2,3] Martin Riccomagno,[1,2] Qiang Wang,[1,2] Lu O. Sun,[1,2] Sarah P. Mitchell,[1,2] Valera Vasioukhin,[4] Richard L. Huganir,[1,2] and Alex L. Kolodkin[1,2]

[1]The Solomon H. Snyder Department of Neuroscience and [2]Howard Hughes Medical Institute, Johns Hopkins University School of Medicine, Baltimore, Maryland 21205, [3]Department of Physiology, Seoul National University School of Dentistry, Seoul, Korea, 110-749, and [4]Division of Human Biology, Fred Hutchinson Cancer research Center, Seattle, Washington 98109

Most excitatory synapses in the mammalian brain are formed on dendritic spines, and spine density has a profound impact on synaptic transmission, integration, and plasticity. Membrane-associated guanylate kinase (MAGUK) proteins are intracellular scaffolding proteins with well established roles in synapse function. However, whether MAGUK proteins are required for the formation of dendritic spines *in vivo* is unclear. We isolated a novel *disc large-5* (*Dlg5*) allele in mice, *Dlg5*^{LP}, which harbors a missense mutation in the DLG5 SH3 domain, greatly attenuating its ability to interact with the DLG5 GUK domain. We show here that DLG5 is a MAGUK protein that regulates spine formation, synaptogenesis, and synaptic transmission in cortical neurons. DLG5 regulates synaptogenesis by enhancing the cell surface localization of *N*-cadherin, revealing a key molecular mechanism for regulating the subcellular localization of this cell adhesion molecule during synaptogenesis.

Key words: **dendritic spine; Dlg5; *N*-cadherin; synaptogenesis**

Introduction

Dendritic spines are the main postsynaptic sites of excitatory synapses in the mammalian brain (Nimchinsky et al., 2002). Spine density, distribution, and morphology exert a profound impact on synaptic transmission, integration, and plasticity (Elston and DeFelipe, 2002; Hayashi and Majewska, 2005; Ballesteros-Yáñez et al., 2006; Knobloch and Mansuy, 2008; Spruston, 2008; Bhatt et al., 2009). Not surprisingly, alterations in spine density and morphology are associated with numerous neurological and psychiatric disorders (Irwin et al., 2000; Kaufmann and Moser, 2000; Knobloch and Mansuy, 2008; Penzes et al., 2011). A comprehensive picture of the molecular and cellular processes that initiate the formation of dendritic spines and synapses requires the identification and functional analysis of the myriad intracellular components required to orchestrate connectivity in the CNS (Lippman and Dunaevsky, 2005; Tada and Sheng, 2006; Yoshihara et al., 2009; Saneyoshi et al., 2010).

A critical early event in dendritic spine formation and synaptogenesis is the stabilization of *trans*-synaptic contacts mediated by cell surface proteins; these proteins include neurexins, neuroligins, ephrins, leucine-rich-repeat proteins, and cadherins (Henkemeyer et al., 2003; Craig and Kang, 2007; Arikkath and Reichardt, 2008; Kayser et al., 2008; Suzuki and Takeichi, 2008; Ko et al., 2009; de Wit et al., 2009; Siddiqui and Craig, 2011). *N*-cadherin is the most abundant and widely distributed classical cadherin in the mammalian brain (Yagi and Takeichi, 2000; Togashi et al., 2002) and its critical role in dendritic spine formation has been well described. For example, in cultured hippocampal neurons, *N*-cadherin knockdown using shRNA results in a decrease in dendritic spine density (Saglietti et al., 2007). However, the intracellular mechanisms that localize *N*-cadherin to the cell surface during dendritic spine formation and synaptogenesis remain poorly understood.

MAGUK proteins are intracellular scaffolding proteins with well established roles in synapse development and function, but whether MAGUK proteins are required for the formation of dendritic spines *in vivo* remains unclear. Discs large homolog 5

Received March 30, 2014; revised July 26, 2014; accepted Aug. 10, 2014.

Author contributions: S.-H.J.W., I.C., R.L.H., and A.L.K. designed research; S.-H.J.W., I.C., S.-Y.C., M.R., Q.W., L.O.S., and S.P.M. performed research; V.V. and R.L.H. contributed unpublished reagents/analytic tools; S.-H.J.W., I.C., S.-Y.C., M.R., Q.W., L.O.S., S.P.M., and A.L.K. analyzed data; S.-H.J.W., I.C., and A.L.K. wrote the paper.

This work was supported by the National Institutes of Health (Grant R01 CA131047 to V.V.) and the Johns Hopkins Brain Science Institute (A.L.K. and R.L.H.). A.L.K. and R.L.H. are investigators of the Howard Hughes Medical Institute. We thank Dan Leahy for help with Dlg-5 protein domain structure evaluation; the Partners Healthcare Center for Genetics and Genomics for performing SNP analysis; the Johns Hopkins University School of Medicine Microscope Facility for assistance with EM analysis; David Ginty and Paul Worley for critically reading the manuscript; Tracy Tran, Janna Merte, Kevin Wright, Qingguang Jiang, Eleftheria Koropouli, and Joshua Jones for helpful discussions; Joshua Jones, Dontais Johnson, and Crystal Chen for technical assistance; and members of the Kolodkin laboratory for assistance throughout the course of this project.

The authors declare no competing financial interests.

Correspondence should be addressed to Dr. Alex L. Kolodkin, Johns Hopkins University School of Medicine, 725 N. Wolfe St., 1001 PCTB725, Baltimore, MD 21205. E-mail: kolodkin@jhmi.edu.

S.-H. Wang's present address: Department of Pathology and Cell Biology, Columbia University Medical Center, New York, NY.

I.C.'s present address: Department of Biochemistry and Molecular Biology, Tulane University School of Medicine, New Orleans, LA.

*S.-H.J.W. and I.C. contributed equally to this work.

DOI:10.1523/JNEUROSCI.1280-14.2014

 0270-6474/14/3412745-17$15.00/0

(DLG5) is a member of the discs large (Dlg) family of MAGUK proteins (de Mendoza et al., 2010). The size and domain organization of DLG5 are distinct from other classical Dlg family members. In addition to the PDZ (PDZ-95, Dlg, ZO-1), SH3 (Src Homology 3), and GUK (Guanylate Kinase) domains, Dlg5 also contains an N-terminal CARD (Caspase Activation and Recruitment Domain) domain, a DUF (Domain of Unknown Function) domain, and a coiled-coil domain (Nechiporuk et al., 2007). Previous work shows that DLG5 is important for the delivery and stabilization of cadherin-catenin protein complexes to the plasma membrane of epithelial cells, and loss of Dlg5 *in vivo* leads to disruption of adherens junctions and epithelial cell polarity in *Dlg5*$^{-/-}$ mutant mice (Nechiporuk et al., 2007). How DLG5 might function in other cell types and organ systems is unknown.

We show here that a *Dlg5* allele, *Dlg5*^{LP}, reveals novel neuronal functions of this MAGUK protein. DLG5 promotes dendritic spine formation and synaptogenesis in cortical pyramidal neurons through the facilitation of *N*-cadherin localization to the neuronal cell surface. The DLG5^{LP} mutant protein abolishes key protein domain interactions required for neuronal DLG5 function. These observations lend insight into the function of MAGUK proteins in synaptogenesis and reveal a critical molecular mechanism for regulating the subcellular localization of cell adhesion molecules during synaptogenesis.

Materials and Methods

Mutagenesis and screening. *N*-ethyl-*N*-nitrosourea mutagenesis was performed as described previously (Merte et al., 2010a; Merte et al., 2010b). Briefly, C57BL/6 (B6) male mice were injected with three doses of 100 mg/kg body weight *N*-ethyl-*N*-nitrosourea to induce random mutations throughout the genome. Using a three-generation breeding scheme (Fig. 1*A*), we outbred the mutations into C3H/Hej (C3H) mice and analyzed G3 mice for developmental abnormalities. Freshly dissected P5 mouse brains were fixed in 4% paraformaldehyde (Sigma) overnight and equilibrated in 30% sucrose. Sagittal sections (150 μm) were cut on a Leica sliding microtome. Sections were stained with anti-neurofilament antibody.

Mapping. Genomic DNA from mutant lines was analyzed for a panel of 768 single nucleotide polymorphisms by Partners Healthcare Center for Genetics and Genomics. The genetic lesion responsible for hydrocephalus was mapped to a 7.3Mb region on chromosome 14 between rs6175633 and rs13482117 using standard linkage analysis of single nucleotide polymorphisms between B6 and C3H mice. Additional polymorphisms within this region, D14Mit207, rs3666933, and rs30102223, were analyzed, allowing us to map the genetic lesion to a 3.1 Mb region on chromosome 14 between D14Mit207 and rs30102223, which includes 15 protein-coding genes (Table 1). *Dlg5* was identified as a candidate gene based on phenotypic similarity of our mutant to previously described *Dlg5*$^{-/-}$ mice (Nechiporuk et al., 2007). We sequenced the open reading frame of *Dlg5* and identified a T→C transition in exon26 as the genetic mutation responsible for hydrocephalus in our mutant line. D14Mit207 was analyzed by genotyping with primers TCCAACTAGTCCCCCTCTACTT and CTGTGACTATCTGTACAAGACCTGC, which produces a PCR product of 126 bp in B6 and 104 bp in C3H mice. rs3666933 was analyzed by genotyping with primers TTGTTTCAGCACAGCCCCAGC and TCATCCCTACATCCCCTGTCC, followed by digestion with DpnI; PCR product from C3H, but not B6 mice, can be cut with DpnI. rs30102223 was analyzed by genotyping with primers CATGACTCTCAAGGGATCCACC and ATCCAAGGACAGCTTGAAGATGC, followed by digestion with SphI; PCR product from C3H, but not B6 mice, can be cut with SphI.

Animals. All mice (*Mus musculus*) used in this study were housed in a 12 h light/dark cycle in groups of 2–5 animals per cage, had access to food and water at libitum, and were cared for in accordance with National Institutes of Health guidelines. All research conducted was done with the approval of the Johns Hopkins University Committee on Care and Use of Animals. *Dlg5*$^{null/null}$ mice (Nechiporuk et al., 2007, RRID:MGI_MGI:3758605) and *N-Cad*$^{flox/flox}$ (Kostetskii et al., 2005, RRID:IMSR_JAX:007611) have been described previously and were kept on a mixed 129/B6 background. *Dlg5*$^{LP/LP}$ mice were kept on a mixed B6/C3H background. Both males and females were included in all experiments. All experiments were performed blinded with respect to genotype.

Genotyping. The T→C transition underlying the *Dlg5*^{LP} allele creates a restriction-enzyme-resistant polymorphism. This mutant line is genotyped by amplification of an ~300 bp fragment with primers GGCGAGTGTCACCCTGTGAG and GCCTTTCTTCCTGATATCTGGAG, followed by digestion with PvuII; only a PCR product from the wild-type allele can be cut with PvuII. Genotyping for *Dlg5*$^{-/-}$ mice and *N-cad*$^{flox/flox}$ mice was performed as described previously (Kostetskii et al., 2005; Nechiporuk et al., 2007).

Plasmids. The V5-DLG5 expression construct was described previously (Nechiporuk et al., 2007). This construct was modified to generate V5-DLG5mCherry by inserting the gene encoding mCherry under the control of the CMV promoter. To generate V5-DLG5(L1642P)mCherry, we used overlapping PCR with primers A: GTGAAGGTGCAGAAGGGTTCAGAGC, B: CTGGGCATTCTCATCCgGCTGCCAGGCCATC, C: GATGGCCTGGCAGCcGGATGAGAATGCCCAG, and D: TGTACTCCTGATCGATCTTCTGTGC. Constructs expressing shRNAs targeting *DLG5* and also silencing-resistant DLG5 were constructed using the LEMPRA based system, as described previously (Zhou et al., 2006). shRNA directed against *DLG5* was cloned into the pLLX vector using primers tAGACAGAAGTTGTGGAATT, ttcaagagaAATTCCACAACTTCTGTCTttttttggaac, tcgagttccaaaaaaAGACAGAAGTTGTGGAATT and tctcttgaaAATTCCACAACTTCTGTCTa. The silencing-resistant form of *DLG5* was generated using overlapping PCR primers: A: ACGCGACCAGGTCATCTCCGAGCTG, B: CTCTCAAATTCtACgACcTCgGTCTCCCAC, C: GTGGGAGACcGAgGTcGTaGAATTTGAGAG, and D: CATGCCGGCTAGCATGCCCTGGTGA and cloning the SexAI/NheI fragment into DLG5 in the pLEMPRA vector. Small letters indicate nucleotides that were changed in DLG5 sequence to generate silencing resistant form. Constructs expressing wild-type SH3 domain or SH3 domain harboring the L1642P mutation were generated by PCR using primers atggccggccatagACCATGGGAGACAGCTTCTACATC (forward) and atgGGCGCGCCGAACTCTTGGTCCATCACGTATTTG (reverse); resulting DNA fragments were ligated upstream of the 3X FLAG epitopes in a pCAGGS vector. A construct expressing the GUK domain was generated by PCR using primers atggccggcctGACTCAGTGAGCCTGGCCTATCAG (forward) and atggcgcgccCTATTGTTCTTGACTGACCATGG (reverse), and the resulting DNA fragment was ligated 3′ to the 6X Myc epitopes in the pCAGGS vector. All constructs generated by PCR were verified by sequencing.

In situ *hybridization*. *In situ* hybridization was performed using standard methods. Generation of a *Dlg5* riboprobe has been described previously (Nechiporuk et al., 2007).

Immunohistochemistry. Immunostaining of tissue sections were was performed using standard methods. Primary antibodies used: mouse anti-neurofilament (1:5000; Developmental Studies Hybridoma Bank, catalog #mAb 2H3, RRID:AB_2312571), rabbit anti-Brn2 (1:500; Santa Cruz Biotechnology, catalog #sc-28594, RRID:AB_2167382), rabbit anti-Cux1 (1:500; Santa Cruz Biotechnology, catalog #sc-13024, RRID:AB_2261231), rat anti-Ctip2 (1:500; Abcam, catalog #ab18465, RRID:AB_2064130), and rabbit anti-Tbr1 (1:500; Santa Cruz Biotechnology, catalog #sc-48816, RRID:AB_2287060). Species-specific secondary antibodies (Invitrogen) were used at 1:500. Immunostaining of cultured neurons were performed using standard methods. Primary antibodies used were as follows: chicken anti-GFP (1:1000; Aves Laboratories, catalog #GFP-1020, RRID:AB_10000240), guinea pig anti-vGlut1 (1:1000; Millipore, catalog #AB5905, RRID:AB_2301751), mouse anti-PSD95 (1:500; Millipore, catalog #MABN68, RRID:AB_10807979), rabbit anti-VGAT (1:1000; Synaptic Systems, catalog #131 003, RRID:AB_887869), mouse anti-gephyrin (1:1000; Synaptic Systems, catalog #147 011, RRID:AB_887717), mouse anti-β catenin (1:100; Sigma-Aldrich, catalog #C7207, RRID:AB_476865), mouse anti-V5 (1:500; Invitrogen, catalog #R96025, RRID:AB_159313), and rabbit anti-DsRed (1:1000; Clontech,

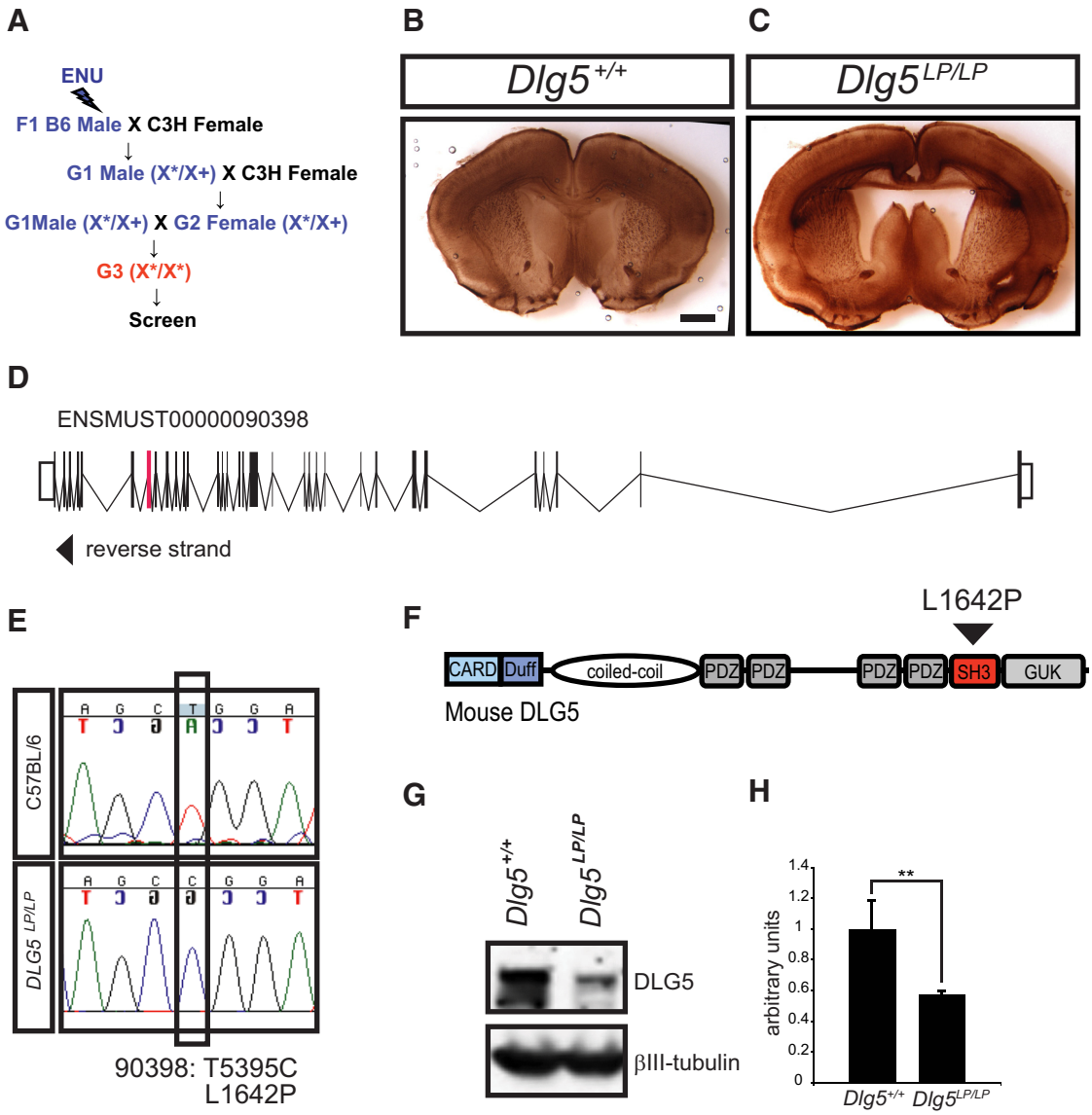

Figure 1. Isolation of the *Dlg5*^{LP} mutant mouse line. ***A***, Breeding scheme for forward genetic screen to identify recessive mutations affecting mammalian brain development. ***B–C***, Neurofilament immunostaining of P5 coronal brain sections of control (***B***) and *Dlg5*^{L1642P} mutant (***C***) littermates showing enlarged lateral ventricles and abnormal corpus callosum. ***D***, Schematic diagram of the *Dlg5* locus highlighting exon 26 (red), in which a single base substitution was identified in the *Dlg5* mutant obtained in our genetic screen. Shown in black are coding exons from the largest predicted *Dlg5* transcript, *ENSMUST00000090398* (Ensembl, RRID:nif-0000–21145). ***E***, Primary DNA sequence data highlighting the *T5395C* mutation in *DLG5* exon 26, resulting in the leucine ^{1642} to proline mutation (*Dlg5*^{LP}). ***F***, Schematic diagram of the DLG5 protein. The L1642P substitution is located within the DLG5 SH3 domain. ***G***, Western-blot analysis of DLG5 protein levels in total brain lysates prepared from *Dlg5*$^{+/+}$ and *Dlg5*$^{LP/LP}$ littermates revealing reduced levels of DLG5 protein in *Dlg5*$^{LP/LP}$ brain lysates. ***H***, Quantification of DLG5 protein levels from the total brain lysates prepared from *Dlg5*$^{+/+}$ and *Dlg5*$^{LP/LP}$ littermates normalized to *Dlg5*$^{+/+}$ protein levels (*Dlg5*$^{+/+}$: 1 ± 0.18; *Dlg5*$^{LP/LP}$: 0.57 ± 0.025). $n = 6$ brains for *Dlg5*$^{+/+}$ and $n = 6$ brains for *Dlg5*$^{LP/LP}$. Error bars indicate SD. $^{**}p < 0.01$ by two-tailed Student's *t* test. Scale bars: 1 mm for ***B*** and ***C***.

catalog #632496, RRID:AB_10013483). Species-specific secondary antibodies (Invitrogen) were used at 1:1000.

In vivo *analysis of dendritic spine density*. A concentrated solution of adeno-associated virus (AAV) expressing eEGFP was injected bilaterally into ventricle of postnatal day 0 (P0)–P2 mice. Dendritic spine quantification was performed on P21 brains. Animals were perfused intracardially with 4% PFA. Dissected brains were then postfixed with 4% PFA, cryoprotected with 30% sucrose, embedded in optimal cutting temperature medium, and sectioned into 100 μm sections on a Leica CM3050 cryostat. Dendritic spines of layer V somatosensory cortex were visualized using immunohistochemistry with anti-GFP antibody (Aves Laboratories) detecting eEGFP.

Golgi analysis. Freshly dissected and P21 mouse brains were incubated in Golgi solution A+B (FD Rapid GolgiStain Kit; FD NeuroTechnologies) for 8 d. After incubation, all brains were washed thoroughly with Solution C for 2–4 d at room temperature and embedded in optimal cutting temperature embedding medium. Coronal sections (100 μm) through the somatosensory cortex and hippocampus were cut with a Leica CM3050 cryostat and mounted on 3% gelatin-coated slides. Staining procedures were followed as described previously (FD NeuroTechnologies) and slides were dehydrated in ethanol, cleared in xylene, and mounted with Permount (Fisher Scientific) for microscopy. Only layer V pyramidal neurons from the somatosensory cortex were included in our analyses.

Primary neuronal cultures. The day of plug was designated embryonic day 0.5 (E0.5) for all timed pregnancies. E13.5 cortices were dissected in ice-cold L-15 Leibovitz medium (Sigma) and incubated in trypsin-EDTA (0.05%; Invitrogen) at 37°C for 15 min. The tissues were washed once at room temperature in Ca^{2+}- and Mg^{2+}- free HBSS (Invitrogen) and dissociated with a fire-polished glass Pasteur pipette in HBSS containing 0.025% DNase I. Dissociated cells were plated on poly-D-lysine (Sigma)-coated 12 mm coverslips at a density of 2×10^5 cells per coverslip and

Table 1. Protein-coding genes between D14Mit207 and rs30102223

cM	Genome coordinates (strand) NCBI Build 37	Symbol, name
12.03	22838934–23875307 (+)	1700112E06Rik, RIKEN cDNA 1700112E06 gene
14.48	25441360–25448422 (+)	4930428N03Rik, RIKEN cDNA 4930428N03 gene
14.47	25425926–25436533 (−)	4930542C16Rik, RIKEN cDNA 4930542C16 gene
14.48	25436790–25440915 (+)	4931403M11Rik, RIKEN cDNA 4931403M11 gene
12.91	24111513–24112865 (−)	A830039N20Rik, RIKEN cDNA A830039N20 gene
14.26	24953175–25065142 (−)	Dlg5, discs, large homolog 5 (Drosophila)
14.33	25112436–25129188 (+)	E330034G19Rik, RIKEN cDNA E330034G19 gene
12.9	23857416–23913793 (−)	Gm10248, predicted gene 10248
14.55	25728900–25732926 (+)	Gm10398, predicted gene 10398
14.31	25057394–25062613 (−)	Gm17105, predicted gene 17105
12.37	23377304–23377675 (−)	Gm5670, predicted gene 5670
14.23	24889296–24889859 (+)	Gm6158, predicted gene 6158
12.92	24117983–24622526 (−)	Kcnma1, potassium large conductance calcium-activated channel, subfamily M, alpha member 1
14.4	25267916–25306268 (−)	Polr3a, polymerase (RNA) III (DNA directed) polypeptide A

grown in 24-well plates in neurobasal medium (Invitrogen) containing 2% B27 supplement (Invitrogen), 50 U/ml penicillin, 50 μg/ml streptomycin (Invitrogen), and 2 mM glutaMAX (Invitrogen) at 37°C with medium changes every other day. Transfection was performed at 8 d in vitro (DIV) with 1 μg of DNA and 2 μl of Lipofectamine (Invitrogen), as described in manufacturer's manual (Invitrogen). After transfection, culture medium was switched to the aforementioned medium plus 2.5% FBS (Invitrogen) and cultured for another 10–13 DIV with medium changes every other day.

In utero *electroporation*. *In utero* electroporation was performed as described previously (Tran et al., 2009). E13.5 embryos from timed-pregnant CD1 female mice were injected using pLLX (control group) or *DLG5* shRNA and then analyzed at P21. Dendritic spines of layer V somatosensory cortex were visualized using immunohistochemistry with anti-GFP antibody (Aves Laboratories) to detect eEGFP encoded by constructs used for electroporation.

Transmission electron microscopy. For transmission electron microscopy (TEM), P21 mice were fixed by transcardial perfusion with 3.0% formaldehyde/1.5% glutaraldehyde in 0.1 M Na^+-cacodylate, 3 mM Ca^{2+}, and 2.5% sucrose, pH 7.4. Brains were dissected and the somatosensory cortex was trimmed and fixed overnight in the aforementioned fixative. The tissue was washed with 0.1 M Na^+-cacodylate/2.5% sucrose, reduced with 2% OsO_4, dehydrated in ethanol, infiltrated, and flat embedded in EPON resin. Semithin and ultrathin sections were collected using a Leica Ultracut microtome and analyzed with a Hitachi 7600 TEM. Only identified synapses on dendritic spines of layer V pyramidal neurons were included in these analyses.

Electrophysiology. Mutant mice and their wild-type littermates 3–4 weeks of age were anesthetized by isoflurane inhalation and decapitated. Brains were quickly dissected in ice-cold buffer containing the following (in mM): 212.7 sucrose, 10 glucose, 2.6 KCl, 1.23 NaH_2PO_4, 26 $NaHCO_3$, 0.5 $CaCl_2$, and 5 $MgCl_2$. Brains were vibratome sectioned in the same solution at 300 μm and transferred to normal ACSF composed of the following (in mM): 124 NaCl, 5 KCl, 1.23 NaH_2PO_4, 26 $NaHCO_3$, 10 glucose, 2 $CaCl_2$, and 1 $MgCl_2$. Slices were recovered at 30°C for 1 h and then maintained at room temperature (22–25°C). Neurons were targeted for whole-cell patch-clamp recording with borosilicate glass electrodes having a resistance of 3–6 MΩ. The electrode internal solution was composed of the following (in mM): 130 cesium methanesulphonate, 10 HEPES, 0.5 EGTA, 8 CsCl, 5 TEA-Cl, 1 QX-314, 10 Na phosphocreatine, 0.5 Na-GTP, and 4 Na-ATP. Cortical pyramidal neurons were selected from layer V of the posterior medial barrel subfield of primary somatosensory cortex. For AMPA receptor-mediated miniature EPSCs, external solution was supplemented with the following: 1 μM tetrodotoxin, 50 μM d,l-APV (2-amino-5-phosphonovalerate), and 100 μM picrotoxin. Data were acquired with a Multiclamp 700A and Clampex 8 program (Molecular Devices) at 10 kHz. Before mEPSC detection and analysis, current traces were low-pass filtered at 1 kHz. mEPSCs were detected and analyzed using Mini Analysis (Synaptosoft) or Clampfit 10 program (Molecular Devices). Kinetic measurements were performed on scaled, mean EPSC traces using a monoexponential decay function. Rise times correspond to 10–90% of peak amplitude. A total of 25 wild-type neurons and 25 mutant neurons were recorded from layer V; $n = 8$ animals for wild-type and $n = 6$ animals for mutant animals.

Subcellular fractionation. Freshly dissected mouse brains were homogenized in ice-cold 4 mM HEPES, pH 7.4, 0.32 M sucrose, and protease inhibitors (Roche). Brain lysates were centrifuged at 2000 $\times$ *g* for 10 min to give S1 (supernatant) and P1 (pellet) fractions. The S1 fraction was centrifuged at 37,000 $\times$ *g* for 30 min to give S2 (supernatant) and P2 (pellet) fractions. The P2 pellet was resuspended in 4 mM HEPES and centrifuged at 82,500 $\times$ *g* for 2 h in a sucrose gradient consisting of 4 mM HEPES plus 0.85 M, 1.0 M, and 1.2 M sucrose. The synaptosomal fraction was harvested at the interface between the 1.2 M and 1.0 M part of the gradient, centrifuged at 150,000 $\times$ *g* for 30 min, and resuspended in 80 mM Tris-HCl, pH 7.8. To isolate postsynaptic density (PSD) fractions, synaptosomes were incubated with 40 mM Tris-HCl, pH 8.0, 0.5% Triton-X for 15 min on ice and then centrifuged at 32,000 $\times$ *g* for 20 min. The pellet was resuspended in 40 mM Tris-HCl, pH 8.0, to give PSD I. The PSD I fraction was incubated again with 40 mM Tris-HCl, pH 8.0, 0.5% Triton-X for 15 min on ice and centrifuged at 201,800 $\times$ *g* for 1 h. The pellet was resuspended in 40 mM Tris-HCl, pH 8.0, with 0.3% SDS to give the PSD II fraction. To isolate the PSD III fraction, PSD I was incubated with 40 mM Tris-HCl, pH 8.0, 3% Sarkosyl for 15 min and centrifuged at 201,800 $\times$ *g* for 1 h. The pellet was resuspended in 40 mM Tris-HCl, pH 8.0, to give PSD III. Protein concentrations were measured by BCA assay (Pierce) and mixed in Laemmli's sample buffer. Western blot analysis was performed on 5 μg of each fraction using standard methods.

Coimmunoprecipitation. For *in vitro* coimmunoprecipitation (co-IP) experiments, HEK293T cells were transfected using Lipofectamine 2000 (Invitrogen) according to the manufacturer's manual. Cells were lysed in RIPA lysis buffer with protease inhibitor (Roche) on ice for 30 min. Cell lysates were precleaned with protein A/G beads before adding rabbit anti-Myc monoclonal antibody (71D10; Cell Signaling Technology, catalog #2278, RRID:AB_490778) for co-IP using standard methods. The co-IP of the SH3 domain was detected with mouse-anti-Flag antibody (M2; Sigma-Aldrich, catalog #F3165, RRID:AB_259529) using standard Western blot methods. For *in vivo* co-IP experiments, freshly dissected mouse brains were homogenized in RIPA lysis buffer with protease inhibitor (Roche) on ice for 30 min. Co-IP was performed using standard methods with mouse anti-β-catenin antibody (1 μg/100 μg of brain lysate, Sigma-Aldrich, catalog #C7207, RRID:AB_476865) and protein A/G agarose beads (Pierce). Coimmunoprecipitated DLG5 and β-catenin were detected using standard Western blot methods.

Surface protein biotinylation assay. Cortical neurons were cultured for 21 DIV and then incubated with 0.5 mg/ml sulfo-NHS-SS-biotin (Pierce) in PBS for 30 min on ice to label cell surface proteins. Unbound biotin was then quenched with 50 mM glycine in PBS. Cells were lysed in RIPA lysis buffer (150 mM NaCl, 1% NP-40, 0.5% deoxycholic acid, 0.2% SDS, 50 mM Tris-HCl, pH 8.0) with protease inhibitor (Roche) and immunocprecipitation of surface protein was performed using standard methods with streptavidin agarose beads (Pierce).

Western blot. Western blot analysis was performed using standard methods. Primary antibodies used were mouse anti-PSD95 (1:2000; Millipore, catalog #MABN68, RRID:AB_10807979), rabbit anti-synaptophysin (1:1000; Santa Cruz Biotechnology, catalog #sc-9 116, RRID:AB_2199007), rabbit anti-GFP (1:1000; Santa Cruz Biotechnology, catalog #sc-33150, RRID:AB_654471), mouse anti-actin (1:5000; Millipore, catalog #CP01–1EA, RRID:AB_566293), mouse anti-β catenin (1:100; Sigma-Aldrich, catalog #C7207, RRID:AB_476865), mouse anti-*N*-cadherin (1:1000; Life Technologies, catalog #333900, RRID:AB_10850887), and mouse anti-GluR1 (1:1000; Huganir laboratory). Generation of rabbit anti-Dlg5 antibody (1:2000) has been described previously (Nechiporuk et al., 2007). Species-specific secondary antibody was used at 1:5000 (Jackson ImmunoResearch).

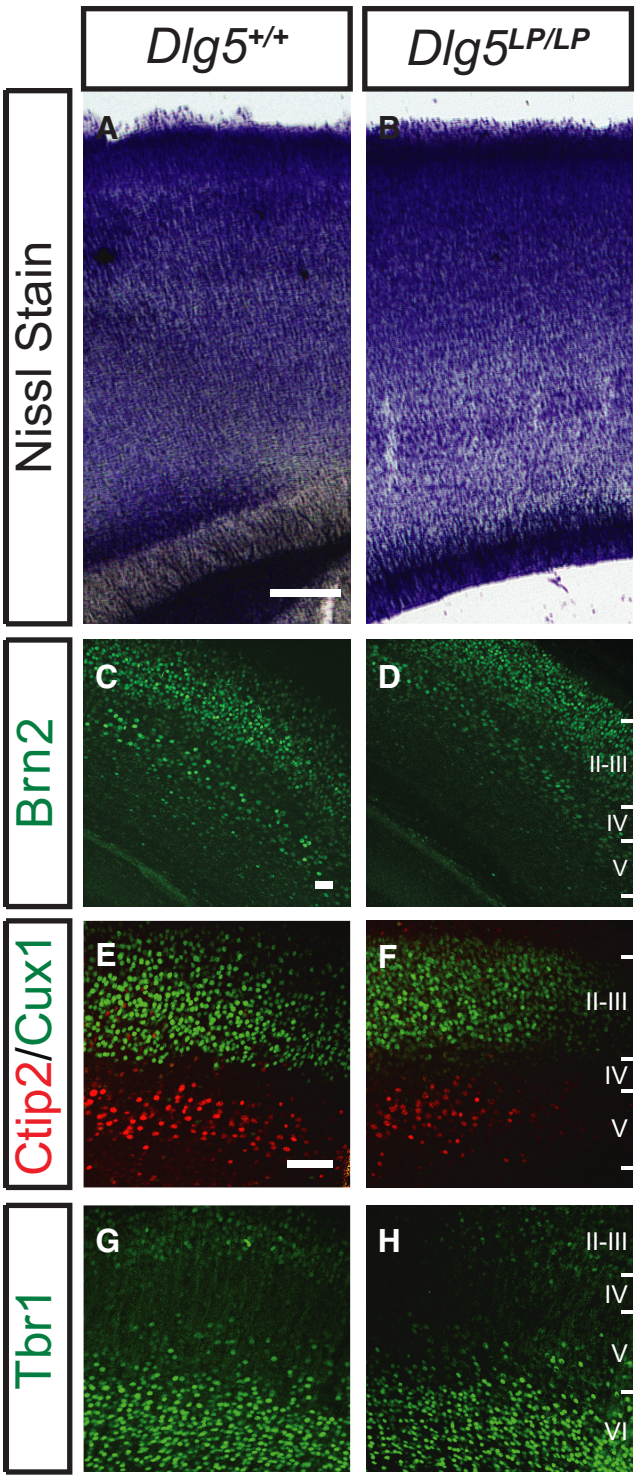

Figure 2. Cortical lamination is normal in *Dlg5* $^{LP/LP}$ mice. ***A–B***, Nissl stain of P5 brain sections from *Dlg5* $^{+/+}$ (***A***) and *Dlg5* $^{LP/LP}$ (***B***) mice. ***C–H***, P5 brain sections from *Dlg5* $^{+/+}$ (***C***, ***E***, ***G***) and *Dlg5* $^{LP/LP}$ (***D***, ***F***, ***H***) mice were stained for Brn2 (***C***, ***D***), Cux1 and Ctip2 (***E***, ***F***), and Tbr1 (***G***, ***H***). *Dlg5* $^{LP/LP}$ mice exhibit apparently normal cerebral cortical lamination. Scale bars: 100 μm for ***A*** and ***B***; 50 μm for ***C***, ***D***, ***E–H***.

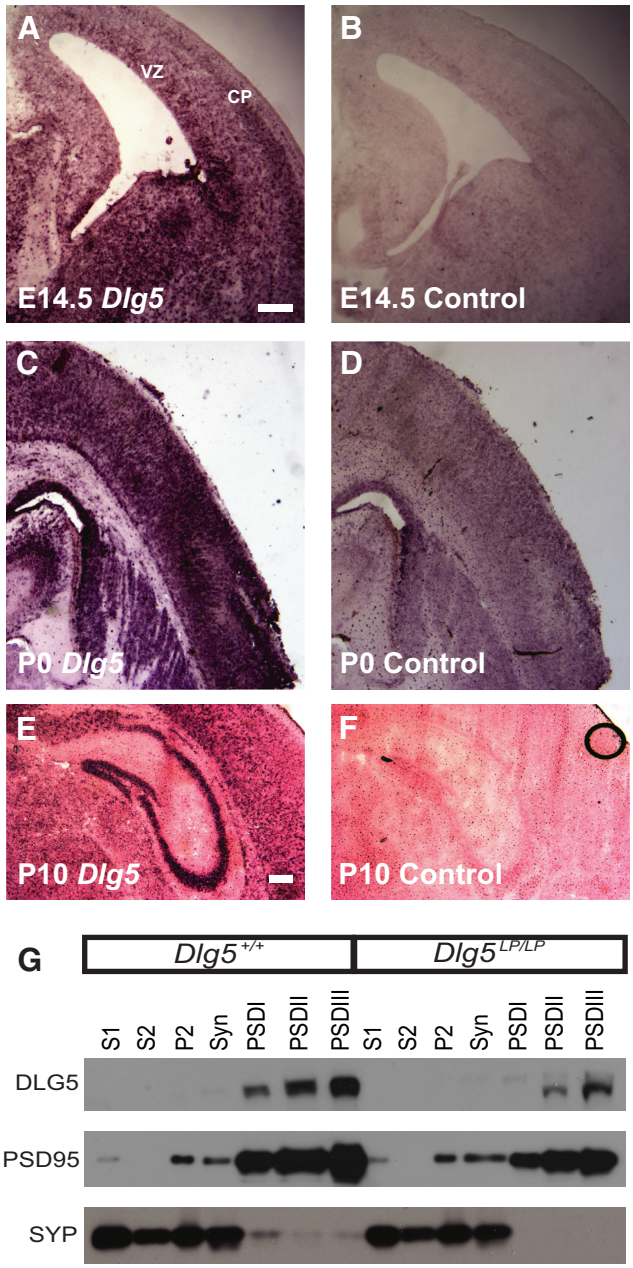

Figure 3. *Dlg5* Is expressed in the postnatal brain and enriched in postsynaptic density fractions. ***A–F***, *In situ* hybridization for *Dlg5* on brain sections from E14.5 (***A***, ***B***), P0 (***C***, ***D***), and P10 (***E***, ***F***) wild-type (WT) mice. Robust expression of *Dlg5* is observed in the ventricular zone (VZ) and cortical plate (CP) at E14.5, cortex and striatum at P0, and cortex and hippocampus at P10. ***A***, ***C***, ***E*** show the antisense probe; ***B***, ***D***, and ***F*** the sense probe (black circle in ***F*** is a bubble on slide). ***G***, Subcellular fractionation of P21 mouse forebrains was performed to generate fractions progressively enriched in synaptic membranes, as verified by immunoblotting for PSD-95 and synaptophysin. DLG5 protein is highly enriched in PSD fractions. DLG5 ^{LP} protein is also enriched in *Dlg5* ^{LP} PSD fractions; however, the protein level is significantly reduced. Scale bars: 200 μm for ***A–D***; 200 μm for ***E*** and ***F***.

Results

A forward genetic screen identifies a novel *Dlg5* allele

Using a three-generation forward genetic screen for recessive mutations affecting murine brain development (Fig. 1*A*; Merte et al., 2010a; Merte et al., 2010b), we identified a mutant mouse line that exhibits severely enlarged ventricles (Fig. 1*B*,*C*). We mapped the genetic lesion underlying this brain defect to a 3.1 Mb interval on chromosome 14 between D14Mit207 and rs30102223 that contains 15 protein-coding genes (Table 1). We identified *Dlg5* as a candidate gene harboring this genetic lesion based on the phenotypic similarity between this mutant and a previously described *Dlg5* $^{-/-}$ mouse mutant (Nechiporuk et al., 2007). We sequenced the open reading frame of *Dlg5* and identified a T→C transition in exon 26 that results in a L1642P missense mutation

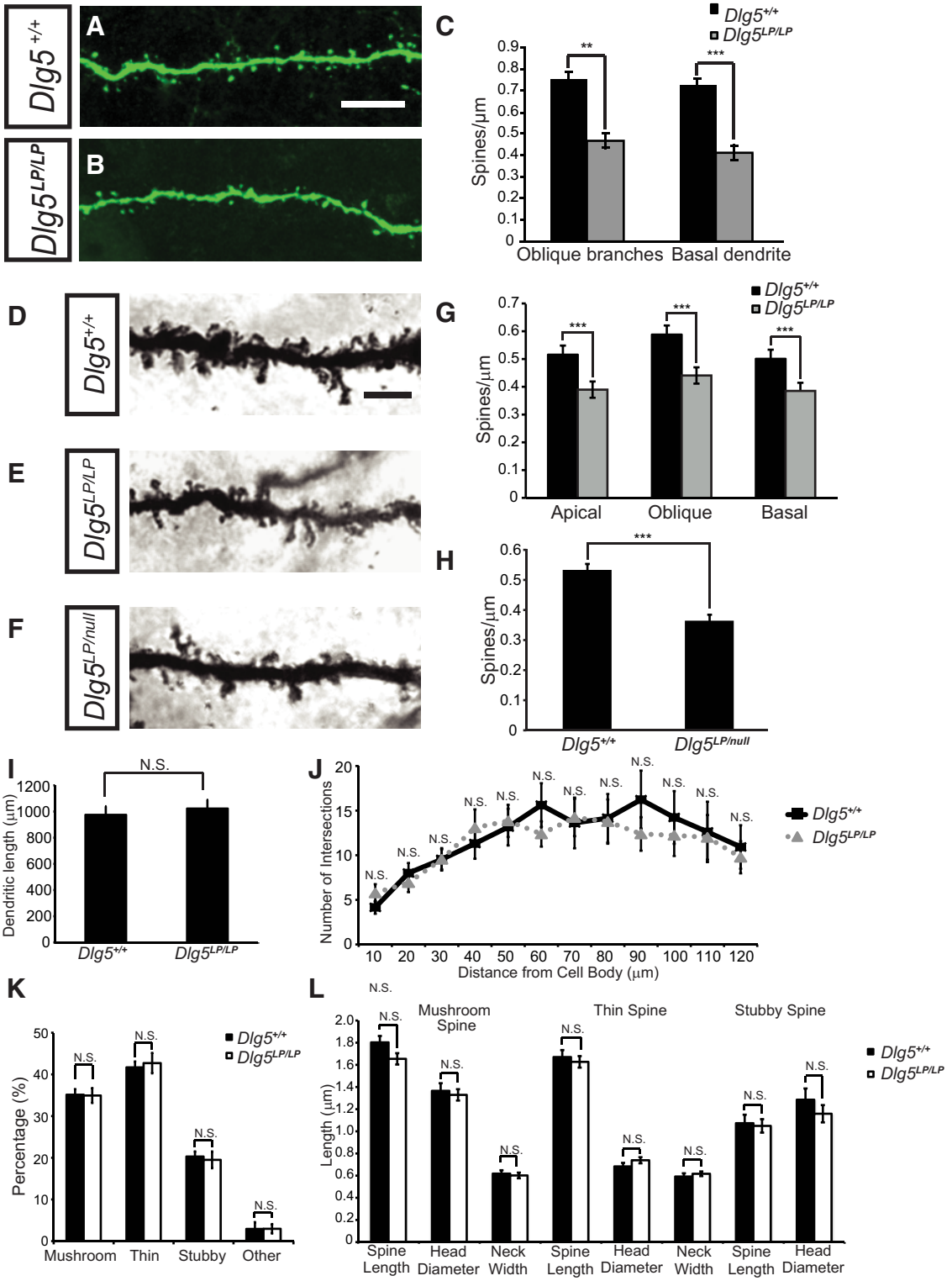

Figure 4. DLG5 regulates dendritic spine density in layer V cortical pyramidal neurons *in vivo*. ***A***, ***B***, Layer V pyramidal neurons from P21 *Dlg5* $^{+/+}$ (***A***) and *Dlg5* $^{LP/LP}$ (***B***) brains were labeled using GFP-expressing AAV. *Dlg5* $^{LP/LP}$ neurons show a significant reduction in dendritic spine density. ***C***, Quantification of dendritic spine density in layer V pyramidal neurons (*Dlg5* $^{+/+}$ side branches: 0.757 ± 0.069 spines/μm; basal dendrites: 0.726 ± 0.028 spines/μm. *Dlg5* $^{LP/LP}$ side branches: 0.467 ± 0.027 spines/μm; basal dendrites: 0.411 ± 0.033 spines/μm). Numbers of neurons quantified: $n = 8$ neurons from 3 brains for *Dlg5* $^{+/+}$; $n = 15$ neurons for oblique branches of the apical dendrite and $n = 10$ for basal dendrites from 5 brains for *Dlg5* $^{LP/LP}$. Error bars indicate SEM. $^{**}p < 0.01$ and $^{***}p < 0.001$ by two-tailed Student's *t* test. ***D–F***, Layer V pyramidal neurons from *Dlg5* $^{+/+}$ (***D***), *Dlg5* $^{LP/LP}$ (***E***), and *Dlg5* $^{LP/null}$ (***F***) brains were examined using Golgi staining at P21. *Dlg5* $^{LP/LP}$ and *Dlg5* $^{LP/null}$ neurons show a significant reduction in dendritic spine density. ***G***, Quantification of dendritic spine density in layer V pyramidal neurons (*Dlg5* $^{+/+}$ apical dendrite: 0.516 ± 0.033 spines/μm; side branches: 0.588 ± 0.033 spines/μm; basal dendrites: 0.501 ± 0.030 spines/μm. *Dlg5* $^{LP/LP}$ apical dendrite: 0.39 ± 0.029 spines/μm; side branches: 0.441 ± 0.029 spines/μm; basal dendrites: 0.385 ± 0.034 spines/μm). Numbers of neurons quantified: $n = 80$ neurons from 5 brains for *Dlg5* $^{+/+}$; $n = 80$ neurons from 6 brains for *Dlg5* $^{LP/LP}$. Error bars indicate SEM. $^{***}p < 0.001$ by two-tailed Student's *t* test. ***H***, Quantification of dendritic spine density in layer V pyramidal neurons (*Dlg5* $^{+/+}$ apical dendrite: 0.532 ± 0.021 spines/μm; *Dlg5* $^{LP/null}$ apical dendrite: 0.364 ± 0.021 spines/μm). Number of neurons quantified: $n = 15$ neurons from 3 brains for *Dlg5* $^{+/+}$; $n = 15$ neurons from 3 brains for *Dlg5* $^{LP/null}$. Error bars indicate SEM. $^{***}p < 0.001$ by two-tailed Student's *t* test. ***I***, Quantification of total dendritic length in layer V pyramidal neurons (*Dlg5* $^{+/+}$: 974.53 ± 65.41 μm; *Dlg5* $^{LP/LP}$: 1022.52 ± 66.76 μm). (*Figure legend continues.*)

in the evolutionarily conserved SH3 domain of the DLG5 protein (Fig. 1*D–F*). We designate this novel *Dlg5* allele *Dlg5*^{LP}. The severity of hydrocephalus in *Dlg5*$^{LP/LP}$ mice is equivalent to that observed in *Dlg5*$^{null/null}$ mice (Nechiporuk et al., 2007). This suggests that the *Dlg5*^{LP} mutant is either a null or a very strong hypomorphic allele of *Dlg5*. Western blot analysis shows that DLG5^{LP} protein is present in *Dlg5*$^{LP/LP}$ mutant brains at ~50% of wild-type DLG5 levels (Fig. 1*G*,*H*). Although *Dlg5*$^{LP/LP}$ mutants exhibit enlarged ventricles, cortical lamination appears normal in these mutants, as revealed by Nissl staining and immunostaining for the cortical layer markers BRN2 (layer II/III, V), CUX1 (layer II/III), CTIP2 (layer V), and TBR1 (layer II/III, VI; Fig. 2).

DLG5 is expressed in the postnatal murine brain

Previous work shows that the hydrocephalus phenotype observed in *Dlg5*$^{-/-}$ mice is caused by disruption of adherens junctions and loss of cell polarity in ventricular epithelial cells, resulting in abnormal closure of the cerebral aqueduct (Nechiporuk et al., 2007). To determine whether DLG5 functions during neural development, we first analyzed *Dlg5* expression in the brain using *in situ* hybridization. We observed strong expression of *Dlg5* mRNA in the cortical plate at E14.5 (Fig. 3*A*,*B*). By P0, *Dlg5* mRNA becomes widely expressed in various regions of the brain, including the cortex, striatum (Fig. 3*C*,*D*), dorsal thalamus, and cerebellum (data not shown). *Dlg5* mRNA expression levels in cortical neurons remain high at P10 (Fig. 3*E*,*F*) and gradually decrease after P21 (data not shown).

To further define DLG5 protein localization, we performed subcellular fractionation of P21 brains to enrich for postsynaptic densities (PSDs), verifying the fidelity of our isolation by immunoblotting for the presynaptic and postsynaptic markers synaptophysin and PSD95, respectively. DLG5 is highly enriched in PSD fractions in wild-type brains and the mutant DLG5^{LP} protein, though present at lower levels than wild-type, retains its localization in the PSD fraction (Fig. 3*G*). These results show that DLG5 is a PSD component and that it is included in the PSD core protein-containing detergent-insoluble PSDIII fraction.

DLG5 regulates dendritic spine density *in vivo*

The strong expression of *Dlg5* in the cerebral cortex during early postnatal development and the localization of DLG5 in PSD fractions raise the possibility that DLG5 may function in cortical neurons. To determine whether DLG5 regulates dendritic spine development *in vivo*, we used GFP-expressing AAV to label and analyze dendritic spine morphology in P21 cortical pyramidal neurons, focusing our analysis on the somatosensory cortex. *Dlg5*$^{LP/LP}$ layer V pyramidal neurons exhibit a 38% and 44% reduction in dendritic spine density along oblique branches of primary apical dendrites and basal dendrites, respectively (Fig. 4*A–C*). This reduction in spine density is not restricted to specific dendritic regions, nor do we observe abnormalities in spine morphology. In a parallel approach, we examined dendritic spine morphology in P21 cortical pyramidal neurons using Golgi staining. Consistent with results obtained using AAV-*GFP* labeling, we observed a significant reduction in dendritic spine density along the primary apical dendrites, oblique branches of apical dendrites, and basal dendrites of *Dlg5*$^{LP/LP}$ layer V pyramidal neurons (Fig. 4*D*,*E*,*G*).

To confirm that the *Dlg5*^{LP} point mutation is the genetic lesion underlying the dendritic spine density phenotype we observed, we performed a complementation test by breeding *Dlg5*$^{LP/LP}$ mice to *Dlg5*$^{null/null}$ mice (Nechiporuk et al., 2007). *Dlg5*$^{LP/null}$ layer V pyramidal neurons show a significant decrease in dendritic spine density (Fig. 4*D*,*F*,*H*). The lack of complementation between *Dlg5*^{LP} and *Dlg5*^{null} alleles shows that the decrease in dendritic spine density is indeed caused by the *Dlg5*^{LP} mutation and not by other, as yet uncharacterized, mutations in the *Dlg5*$^{LP/LP}$ mouse genome.

In contrast to the reduction in dendritic spine density in *Dlg5* mutant mice, we did not observe significant defects in total dendritic length (Fig. 4*I*), basal dendrite complexity (Fig. 4*J*), or dendritic spine morphology (Fig. 4*K*,*L*) in *Dlg5*$^{LP/LP}$ and *Dlg5*$^{null/null}$ mice (data not shown). These findings suggest that DLG5 regulates dendritic spine formation without affecting other aspects of dendritic development and spine morphogenesis.

DLG5 regulates dendritic spine development cell autonomously

To eliminate the possibility that reduction in dendritic spine density is a secondary consequence of enlarged ventricles, we next examined dendritic spine density in cultured cortical pyramidal neurons. Cortical neurons were derived from E13.5 embryos, transfected with a DNA construct expressing GFP at 8 DIV to visualize dendritic spines, and then cultured for a total of 18 DIV. Enlargement of the lateral ventricles is not observed in *Dlg5* mutants at E13.5, the developmental time point when cortical neurons are dissected from the mouse embryo and placed in culture (data not shown). Consistent with our *in vivo* observations, *Dlg5*$^{LP/LP}$ pyramidal neurons *in vitro* show a 25% reduction in spine density (Fig. 5*A–C*). These results strongly suggest that the *Dlg5*$^{LP/LP}$ dendritic spine phenotype we observed *in vivo* does not result from the progressive enlargement of lateral ventricles that occurs in these mutants or from any other defects associated with *Dlg5*^{LP}. Furthermore, *Dlg5*$^{null/null}$ pyramidal neurons *in vitro* also show a 25% reduction in spine density (Fig. 5*D–F*), equivalent to that observed in *Dlg5*$^{LP/LP}$ neurons. This confirms that the *Dlg5*^{LP} mutant is a null, or very strong loss-of-function, *Dlg5* allele.

The enrichment of the DLG5 protein in PSD fractions raises the possibility that DLG5 functions cell autonomously in postsynaptic neurons to regulate dendritic spine formation and synaptogenesis. To test this idea, we designed shRNA constructs that

←

(*Figure legend continued.*) There is no significant difference in total dendritic length. Number of neurons quantified: $n = 13$ neurons from 5 brains for *Dlg5*$^{+/+}$; $n = 13$ neurons from 5 brains for *Dlg5*$^{LP/LP}$. Error bars indicate SEM. N.S. $p = 0.612$ by two-tailed Student's *t* test. ***J***, Sholl analysis of layer V pyramidal neuron basal dendritic arbors shows no significant difference in dendritic complexity. Number of neurons quantified: $n = 13$ neurons from 5 brains for *Dlg5*$^{+/+}$; $n = 13$ neurons from 5 brains for *Dlg5*$^{LP/LP}$. Error bars indicate SEM. N.S. $p > 0.05$ by two-tailed Student's *t* test. ***K***, Percentage of different classes of spines (*Dlg5*$^{+/+}$ mushroom spine: 35.1 ± 1.3%, thin spine: 41.7 ± 1.4%, stubby spine: 20.3 ± 1.2%, others: 2.9 ± 1.6%; *Dlg5*$^{LP/LP}$ mushroom spine: 34.9 ± 1.8%, thin spine: 42.7 ± 2.5%, stubby spine: 19.5 ± 2.0%, others: 2.9 ± 1.1%). There is no significant difference in the percentage of different classes of spines. Number of neurons quantified: $n = 15$ neurons from 5 brains for *Dlg5*$^{+/+}$; $n = 15$ neurons from 5 brains for *Dlg5*$^{LP/LP}$. Error bars indicate SEM. N.S. $p > 0.05$ by two-tailed Student's *t* test. ***L***, Morphologic analysis of different classes of spines (*Dlg5*$^{+/+}$ mushroom spine length: 1.803 ± 0.058 μm, head diameter: 1.365 ± 0.069 μm, neck width: 0.618 ± 0.030 μm, thin spine length: 1.670 ± 0.063 μm, head diameter: 0.683 ± 0.032 μm, neck width: 0.592 ± 0.029 μm, stubby spine length: 1.073 ± 0.077 μm, head diameter: 1.285 ± 0.101 μm; *Dlg5*$^{LP/LP}$ mushroom spine length: 1.654 ± 0.051 μm, head diameter: 1.329 ± 0.051 μm, neck width: 0.602 ± 0.025 μm, thin spine length: 1.627 ± 0.052 μm, head diameter: 0.739 ± 0.028 μm, neck width: 0.617 ± 0.021 μm, stubby spine length: 1.049 ± 0.061 μm, head diameter: 1.159 ± 0.078 μm). Number of spines quantified: $n = 56$ mushroom spines, 67 thin spines, and 33 stubby spines from 15 neurons from 5 brains for *Dlg5*$^{+/+}$; $n = 53$ mushroom spines, 71 thin spines, and 31 stubby spines from 15 neurons from 5 brains for *Dlg5*$^{LP/LP}$. Error bars indicate SEM. N.S. $p > 0.05$ by two-tailed Student's *t* test. Scale bars: 10 μm for ***A*** and ***B***, 5 μm for ***D–F***.

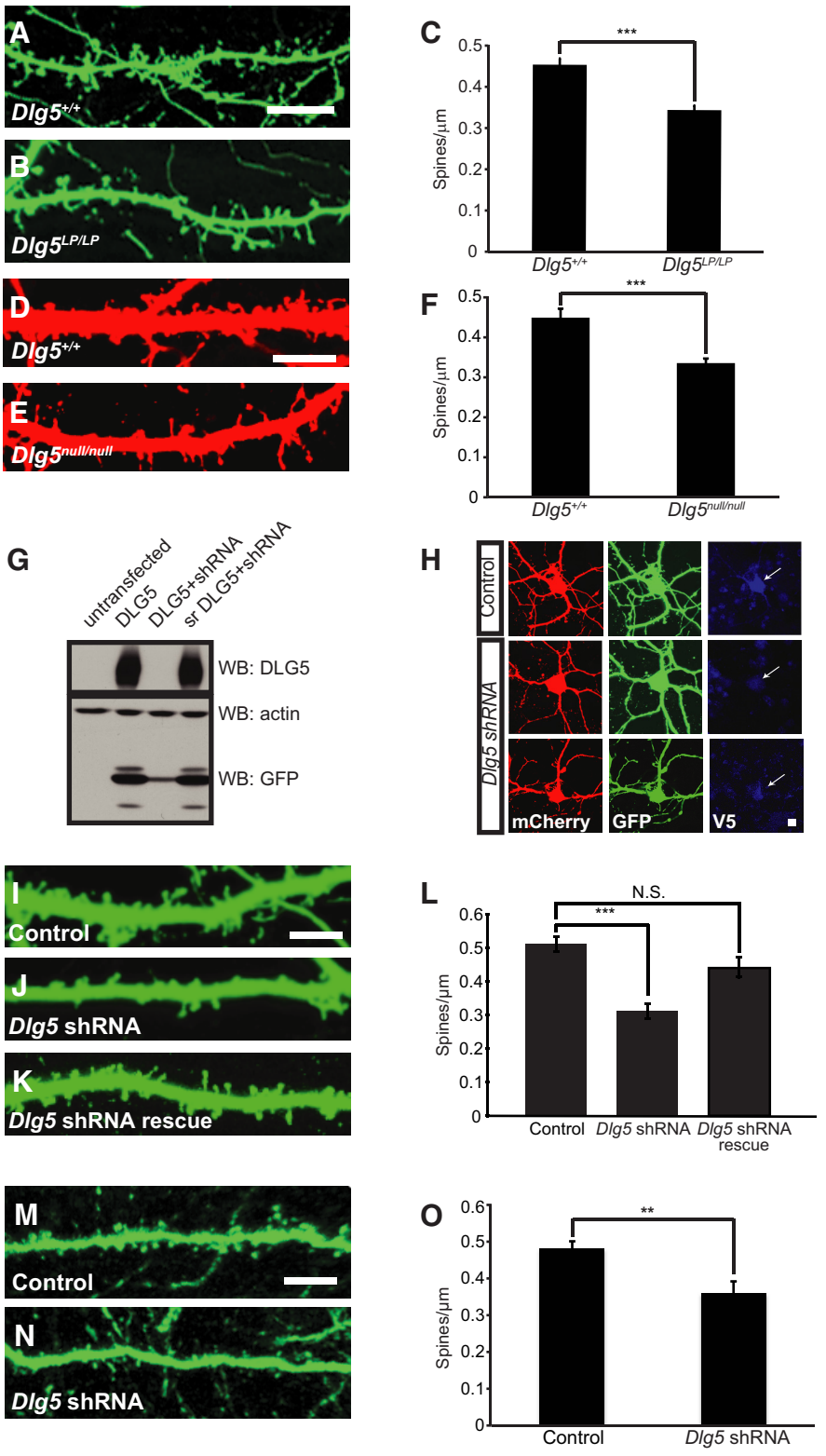

Figure 5. DLG5 regulates dendritic spine density cell autonomously. ***A***, ***B***, Cortical neurons derived from E13.5 *Dlg5* $^{+/+}$ (***A***) and *Dlg5* $^{LP/LP}$ (***B***) embryos were cultured for 8 DIV, transfected with a GFP-expressing construct to visualize dendritic spines, and cultured for a total of 18 DIV. *Dlg5* $^{LP/LP}$ cortical neurons with pyramidal morphology show a significant reduction in dendritic spine density *in vitro*. ***C***, Quantification of dendritic spine density in cultured cortical neurons at 18 DIV (*Dlg5* $^{+/+}$: 0.454 ± 0.015 spines/μm; *Dlg5* $^{LP/LP}$: 0.345 ± 0.011 spines/μm). Number of neurons quantified: $n = 39$ neurons from 3 independent cultures for *Dlg5* $^{+/+}$, and $n = 60$ neurons from 3 independent cultures for *Dlg5* $^{LP/LP}$. Error bars indicate SEM. ***$p < 0.001$ by two-tailed Student's *t* test. ***D***, ***E***, Cortical neurons derived from E13.5 *Dlg5* $^{+/+}$ ***D***, and *Dlg5* $^{null/null}$ ***E***, embryos were transfected with GFP at 8 DIV to visualize dendritic spines and cultured for a total of 18 DIV. *Dlg5* $^{-/-}$ mutant neurons show a significant reduction in dendritic spine density. ***F***, Quantification of dendritic spine density in cultured cortical neurons at 18 DIV (*Dlg5* $^{+/+}$: 0.449 ± 0.022 spines/μm; *Dlg5* $^{null/null}$: 0.336 ± 0.011 spines/μm). Number of neurons quantified: $n = 20$ neurons from 3 independent cultures for *Dlg5* $^{+/+}$, and $n = 20$ neurons from 3 independent cultures for *Dlg5* $^{null/null}$. Error bars indicate SEM. ***$p < 0.001$ by two-tailed Student's *t* test. ***G***, Western-blot analysis of whole-cell extracts prepared from HEK293T cells transfected with constructs expressing GFP-IRES-*Dlg5*, shRNA targeting *Dlg5* and a silencing resistant *Dlg5* shRNA (*srDLG5*). Immunoblotting with DLG5 antibody demonstrates efficient reduction in DLG5 protein levels in extracts prepared from cells transfected with the *Dlg5* shRNA construct and no reduction after transfection with *srDLG5*. Actin provides the loading control. ***H***, Cortical neurons derived from E13.5 embryos were transfected with constructs expressing GFP and V5-*Dlg5-mCherry*, or GFP, *Dlg5* shRNA and V5-*Dlg5-mCherry*, at 8 DIV and cultured for a total of 18 DIV. Immunostaining for V5 (blue) shows efficient reduction in DLG5 protein levels in neurons transfected with *Dlg5* shRNA. ***I–K***, Cortical neurons derived from E13.5 wild-type embryos were transfected with constructs expressing GFP (***I***), *Dlg5* shRNA (***J***), and *srDlg5* (***K***) at 8 DIV and cultured for a total of 18–21 DIV. *Dlg5* knockdown with *Dlg5* shRNA resulted in a significant reduction in dendritic spine density, which was suppressed by *srDlg5*. ***L***, Quantification of dendritic spine density in cultured cortical neurons at 18–21 DIV. (GFP: 0.455 ± 0.029 spines/μm; *Dlg5* shRNA and GFP: 0.257 ± 0.024 spines/μm; *srDlg5* shRNA and GFP: 0.417 ± 0.024 spines/μm). Number of neurons quantified: $n = 15$ neurons from 3 independent cultures for GFP, $n = 15$ neurons from 3 independent cultures for *Dlg5* shRNA, and $n = 16$ neurons from 3 independent cultures for *Dlg5* shRNA rescue. Error bars indicate SEM. ***$p < 0.001$ and N.S. $p = 0.313$ by two-tailed Student's *t* test. ***M***, ***N***, Layer V cortical neurons of wild-type mice were sparsely transfected with GFP (***M***) or *Dlg5* shRNA (***N***) by *in utero* electroporation at E13.5 and analyzed by GFP immunostaining at P21. *Dlg5* knockdown using shRNA resulted in a significant reduction in dendritic spine density *in vivo*. ***O***, Quantification of dendritic spine density in cortical neurons labeled by *in utero* electroporation at P21 (GFP: 0.481 ± 0.02 spines/μm. *Dlg5* shRNA: 0.359 ± 0.033 spines/μm). Number of neurons quantified: $n = 10$ neurons for GFP, and $n = 10$ neurons for *Dlg5* shRNA. Error bars indicate SEM. **$p < 0.01$ by two-tailed Student's *t* test. Scale bar in 10 μm for ***A*** and ***B***, 7.5 μm for ***D*** and ***E***, 10 μm for ***I–K***, and 10 μm for ***M*** and ***N***.

reduce DLG5 protein to nearly undetectable levels in HEK293T cells (Fig. 5*G*) and also in cultured cortical neurons (Fig. 5*H*). Wild-type cortical neurons derived from E13.5 embryos were transfected with *Dlg5* shRNA at 8 DIV and cultured for a total of 18–21 DIV. shRNA knockdown of *Dlg5* causes a 39% reduction in dendritic spine density (Fig. 5*I*,*J*,*L*). To eliminate the possibility of *Dlg5* shRNA off-target effects, we designed a construct that expresses an shRNA silencing-resistant *Dlg5* together with the *Dlg5* shRNA (Fig. 5*G*). Cortical neurons transfected with this rescue construct show wild-type dendritic spine densities (Fig. 5*I*,*K*,*L*), confirming that the shRNA phenotype we observe is indeed caused by *DLG5* loss-of-function.

To assess cell autonomous *DLG5* requirements *in vivo*, we performed *in utero*

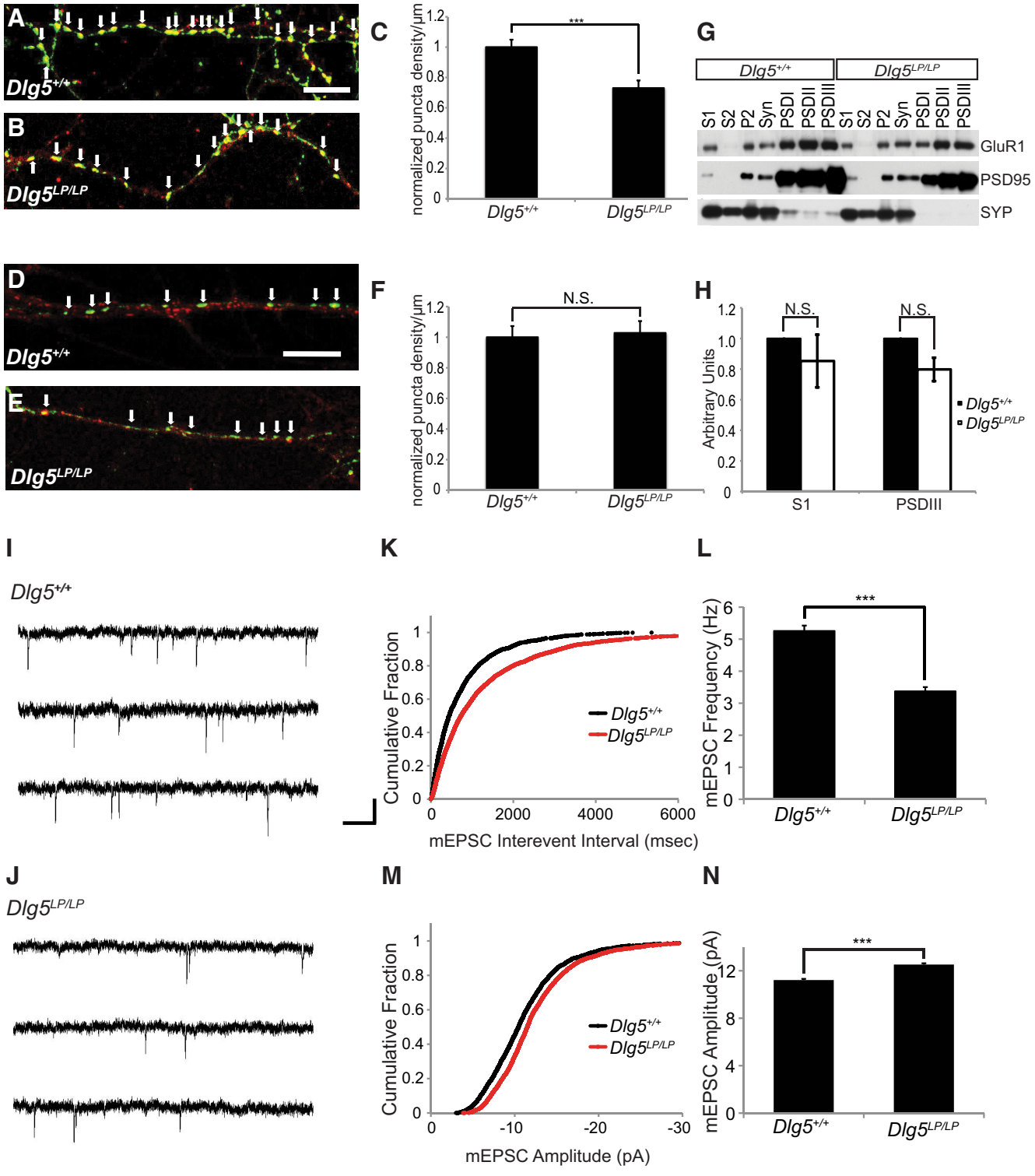

Figure 6. DLG5 regulates excitatory synapse density. ***A***, ***B***, Cortical neurons derived from E13.5 *Dlg5* $^{+/+}$ (***A***) and *Dlg5* $^{LP/LP}$ (***B***) embryos were cultured for 21 DIV. Excitatory synapses were visualized using antibodies recognizing vGlut1 (green) and PSD95 (red), presynaptic and postsynaptic markers, respectively. Colocalized vGlut1/PSD95 puncta indicate excitatory synapses (white arrows). *Dlg5* $^{LP/LP}$ neurons show significant reduction in excitatory synapse density. Shown are representative images for *Dlg5* $^{+/+}$ (***A***) and *Dlg5* $^{LP/LP}$ (***B***) dendritic segments. ***C***, Quantification of excitatory synapses from *Dlg5* $^{+/+}$ and *Dlg5* $^{LP/LP}$ cultured neurons. Values are normalized to *Dlg5* $^{+/+}$ neurons: *Dlg5* $^{+/+}$: 1 ± 0.049 vGlut1/PD95 colocalized puncta/μm; *Dlg5* $^{LP/LP}$: 0.729 ± 0.05 vGlut1/PSD95 colocalized puncta/μm. Number of neurons quantified: $n = 23$ neurons from 3 independent cultures for *Dlg5* $^{+/+}$, and $n = 30$ neurons from 3 independent cultures for *Dlg5* $^{LP/LP}$. Error bars indicate SEM. ***$p < 0.001$ by two-tailed Student's *t* test. ***D***, ***E***, Cortical neurons derived from E13.5 *Dlg5* $^{+/+}$ (***D***) and *Dlg5* $^{LP/LP}$ (***E***) embryos were cultured for 21 DIV. Inhibitory synapses were visualized using antibodies that recognize VGAT (green) and gephryn (red), presynaptic and postsynaptic inhibitory markers, respectively. Colocalized VGAT/gephryn puncta indicate inhibitory synapses (white arrows). *Dlg5* $^{LP/LP}$ neurons show no reduction in inhibitory synapse density. Representative images for *Dlg5* $^{+/+}$ (***D***) and *Dlg5* $^{LP/LP}$ (***E***) dendritic segments are shown. ***F***, Quantification of inhibitory synapse density from *Dlg5* $^{+/+}$ and *Dlg5* $^{LP/LP}$ cultured cortical neurons. Values are normalized to *Dlg5* $^{+/+}$ neurons: *Dlg5* $^{+/+}$: 1 ± 0.073 VGAT/gephryn colocalized puncta/μm; *Dlg5* $^{LP/LP}$: 1.028 ± 0.077 VGAT/gephryn colocalized puncta/μm. Number of neurons quantified: $n = 18$ neurons from 3 independent cultures for *Dlg5* $^{+/+}$, and $n = 19$ neurons from 3 independent cultures for *Dlg5* $^{LP/LP}$. Error bars indicate SEM. N.S. $p = 0.794$ by two-tailed Student's *t* test. ***G***, Western blot analysis of GluR1 in synaptic fractions of (*Figure legend continues.*)

electroporation of wild-type E13.5 brains using our *Dlg5* shRNA construct and a GFP-expressing control construct. At P21, layer V cortical neurons electroporated with *Dlg5* shRNA show a 25% reduction in dendritic spine density compared with neurons electroporated with the GFP control (Fig. 5*M–O*). In cultured cortical neurons and also in the electroporated brains, only a very small number of neurons receive the *Dlg5* shRNA construct, resulting in single, isolated, DLG5-negative neurons surrounded by wild-type neurons and glia. These results demonstrate that DLG5 functions cell autonomously in postsynaptic neurons to regulate dendritic spine development. Given that our shRNA acutely downregulates DLG5 protein expression, these results further suggest that the reduction in dendritic spine density observed in $Dlg5^{LP/LP}$ mutants is due to a lack of neuronal DLG5 function and does not result from progressive enlargement of lateral ventricles.

Dlg5 mutants exhibit decreased excitatory synapse density and altered synaptic properties

Dendritic spines are sites of excitatory synaptic contact (Nimchinsky et al., 2002). To investigate whether there is a corresponding change in excitatory synapse number in $Dlg5^{LP/LP}$ mice, we first analyzed synapse density in cultured cortical neurons by immunostaining with synaptic markers. Cortical neurons from E13.5 embryos were cultured for 21 DIV and then stained for the excitatory presynaptic marker vGlut1 and the postsynaptic marker PSD95. Colocalization of vGlut1 and PSD95 puncta was then determined to assess excitatory synapse number. Consistent with our dendritic spine analysis, we observed a 27% decrease in vGlut1/PSD95 double-positive puncta in dendrites of cultured $Dlg5^{LP/LP}$ neurons (Fig. 6*A–C*). In addition, we stained cultured cortical neurons for the inhibitory presynaptic marker VGAT and the postsynaptic marker gephyrin. We observed no change in VGAT/gephyrin double-positive puncta in cultured $Dlg5^{LP/LP}$ cortical neurons (Fig. 6*D–F*), suggesting that DLG5 does not affect inhibitory synaptogenesis.

Glutamate receptors are the predominant excitatory neurotransmitter receptor in the mammalian brain and MAGUK proteins, including PSD95, regulate AMPA receptor localization and trafficking (Kim and Sheng, 2004). To investigate whether DLG5 has a similar role in regulating synaptic localization of AMPA receptors, we performed Western blot analysis of GluR1 in subcellular fractions prepared from P21 $Dlg5^{+/+}$ and $Dlg5^{LP/LP}$ forebrain lysates. We observe no significant difference in the amount or distribution of GluR1 in postsynaptic density fractions (Fig. 6*G*,*H*). These results suggest that DLG5 regulates excitatory synapse density without affecting synaptic glutamate receptor levels.

To investigate the functional consequences of decreased excitatory synapse density in $Dlg5^{LP/LP}$ mutants, we performed whole-cell patch-clamp recordings of layer V cortical neurons in cortical slices derived from P21–P28 mice. mEPSC analysis revealed a 36% reduction in mEPSC frequency in $Dlg5^{LP/LP}$ neurons (Fig. 6*I–L*). The altered cortical morphology that results from the enlarged cortical ventricles at P21 in $Dlg5^{LP/LP}$ mutant brains precluded performing paired-pulse recordings from layer V cortical neurons. Nevertheless, we show that DLG5 functions cell autonomously in postsynaptic neurons to regulate dendritic spine density (Fig. 5) and $Dlg5^{LP/LP}$ neurons have normal presynaptic terminal morphology as assessed by TEM analysis (see next paragraph). Therefore, the reduction in mEPSC frequency in $Dlg5^{LP/LP}$ neurons most likely results from decreased numbers of excitatory synapses rather than a decrease in presynaptic release probability. There was a slight increase of ~10% in mEPSC amplitude in $Dlg5^{LP/LP}$ neurons (Fig. 6*M*,*N*). We did not observe a significant difference in the levels of synaptic AMPA receptors in $Dlg5^{LP/LP}$ brains (Fig. 6*G*,*H*); therefore, this modest increase in mEPSC amplitude could be due to other compensatory mechanisms or as yet unidentified molecular interactions involving DLG5 that affect glutamate receptor function. These results reveal a significant reduction in excitatory synaptic transmission onto layer V cortical neurons in $Dlg5^{LP/LP}$ mice, consistent with our observation of a reduction in the number of excitatory synapses in these mutants.

To investigate the effects of the $Dlg5^{LP}$ mutation on spine morphology and synapse formation *in vivo*, we used TEM to analyze $Dlg5^{LP/LP}$ cortical neurons at high resolution. In agreement with our *in vitro* observations, we found a 25% decrease in synapse density in layer V $Dlg5^{LP/LP}$ cortical neurons (Fig. 7*A*,*B*,*E*); however, excitatory synapse morphology was apparently normal (Fig. 7*C*,*D*). Quantification of spine area, PSD length, synaptic vesicle number per terminal, and synaptic vesicle diameter (Fig. 7*F–I*) shows that synapses in the $Dlg5^{LP/LP}$ cortex are indistinguishable from those observed in wild-type. These results suggest that DLG5 is involved primarily in initial synapse formation, but not subsequent synaptic maturation or remodeling.

The $DLG5^{L1642P}$ SH3 domain mutation disrupts interactions between the DLG5 SH3 and GUK domains

Although DLG5 protein levels in the $Dlg5^{LP/LP}$ mutant brain are reduced by ~50%, the reduction in $Dlg5^{LP/LP}$ dendritic spine density is comparable to that observed in $Dlg5^{null/null}$ mice (Fig. 4*J–L*), suggesting that the *L1642P* mutation affects the normal function of DLG5. The L1642P point mutation lies within the DLG5 SH3 domain, a domain also present in other MAGUK proteins including PSD95 (Kim and Sheng, 2004). The PSD95 SH3 domain structure differs greatly from canonical SH3 domains, lacking the characteristic secondary structure required for interactions with proline-rich motifs (McGee et al., 2001). Instead, the PSD95 SH3 domain binds to its own GUK domain in an intramolecular fashion and this interaction may be important for the regulated assembly of PSD95 oligomers or the formation of protein conformations essential for interactions with other cell surface proteins and signaling molecules (McGee and Bredt, 1999; McGee et al., 2001; Tavares et al., 2001). In the crystal

←

(*Figure legend continued.*) $Dlg5^{+/+}$ and $Dlg5^{LP/LP}$ brains. Subcellular fractionation of P21 mouse forebrains was performed to generate fractions progressively enriched in synaptic membranes, as verified by immunoblotting for PSD-95 and synaptophysin. There is no significant difference in the level and distribution of GluR1. ***H***, Quantification of GluR1 protein levels from S1 and PSD fractions prepared from $Dlg5^{+/+}$ and $Dlg5^{LP/LP}$ littermates, normalized to $Dlg5^{+/+}$ protein levels ($Dlg5^{LP/LP}$ S1: 0.85 ± 0.172, PSDIII: 0.80 ± 0.076). $n = 3$ brains for $Dlg5^{+/+}$ and $n = 3$ brains for $Dlg5^{LP/LP}$. Error bars indicate SEM. N.S. $p = 0.482$ (S1) and $p = 0.118$ (PSDIII) by two-tailed Student's *t* test. ***I***, ***J***, Layer V cortical neuron mEPSCs were recorded from $Dlg5^{+/+}$ and $Dlg5^{LP/LP}$ somatosensory cortical slices. Sample traces from $Dlg5^{+/+}$ (***G***) and $Dlg5^{LP/LP}$ (***H***) are shown. ***K***, The cumulative plot shows an increase in mEPSC interevent interval in $Dlg5^{LP/LP}$ layer V cortical neurons. Statistically significant by Kolmogorov-Smirnoff test. ***L***, mEPSC frequency is reduced in $Dlg5^{LP/LP}$ layer V cortical neurons ($Dlg5^{+/+}$: 5.254 ± 0.17 Hz; $Dlg5^{LP/LP}$: 3.37 ± 0.132 Hz.). Number of neurons recorded: $n = 25$ neurons from 8 mice for $Dlg5^{+/+}$, and $n = 25$ neurons from 6 mice for $Dlg5^{LP/LP}$. Error bars indicate SEM. ***$p < 0.001$ by two-tailed Student's *t* test. ***M***, The cumulative plot shows a modest but significant increase in mEPSC amplitude in $Dlg5^{LP/LP}$ layer V cortical neurons. Statistically significant by Kolmogorov-Smirnoff test. ***N***, mEPSC amplitude is modestly increased in $Dlg5^{LP/LP}$ layer V cortical neurons ($Dlg5^{+/+}$: 11.216 ± 0.01 pA; $Dlg5^{LP/LP}$: 12.523 ± 0.106 pA). Error bars indicate SEM. ***$p < 0.001$ by two-tailed Student's *t* test. Scale bars: 10 μm for ***A*** and ***B***, 10 μm for ***D*** and ***E***.

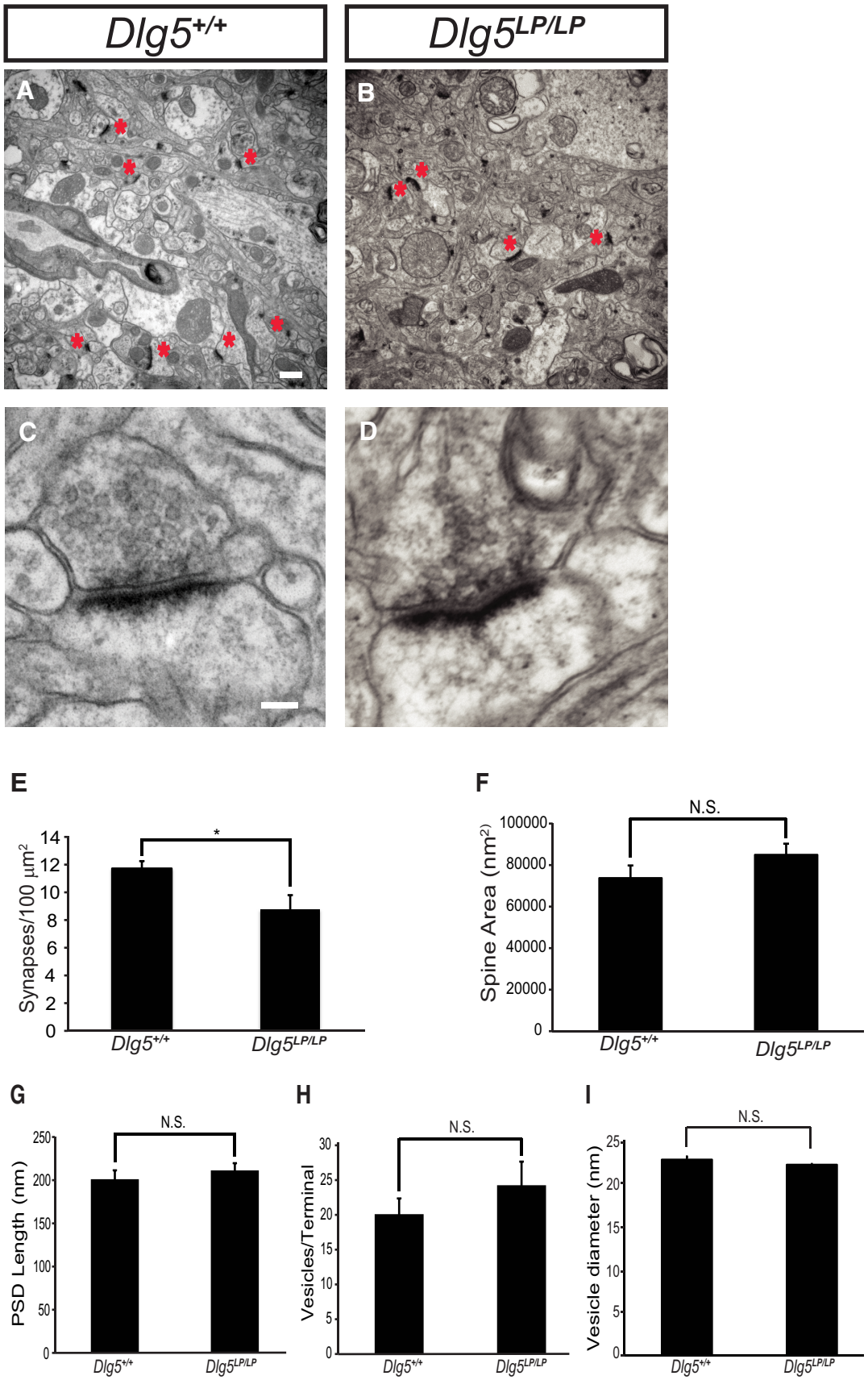

Figure 7. Ultrastructural analysis shows decreased excitatory synapse density but normal synapse morphology in *Dlg5* $^{LP/LP}$ mice. ***A***, ***B***, TEM analysis of layer V cerebral cortex at P21 reveals a significant reduction in excitatory synapse density in *Dlg5* $^{LP/LP}$ brains (***A***) compared with *Dlg5* $^{+/+}$ brains (***B***). Red asterisks represent excitatory synapses. ***C***, ***D***, Higher-magnification TEM views of of *Dlg5* $^{+/+}$ (***C***) and *Dlg5* $^{LP/LP}$ (***D***) cortical neuron dendritic spines. Synapse morphology appears normal in *Dlg5* $^{LP/LP}$ mice. ***E***, Quantification of excitatory synapse (*Figure legend continues.*)

structure of the related MAGUK protein human Z0–1 (Nomme et al., 2011), isoleucine562 in the SH3 domain, which is homologous to leucine1642 in DLG5, is positioned ~4.3 A from tryptophan799 in the GUK domain and these two residues make contact within the hydrophobic core (Fig. 8*A*). The close proximity of this amino acid pair suggests that leucine1642 in the DLG5 SH3 domain may be important for interactions between the DLG5 SH3 and GUK domains. Conformational rigidity of the proline that replaces the leucine in the DLG5^{LP} mutant could destabilize this interaction. Given the position of leucine1642 at the binding interface between the SH3 and GUK domains, we investigated whether the DLG5 SH3 domain binds to the DLG5 GUK domain and if the L1642P mutation disrupts this interaction. We cotransfected HEK293T cells with a construct expressing FLAG-tagged DLG5 WT or L1642P SH3 domains and a construct expressing MYC-tagged DLG GUK. Immunoprecipitation of cell lysates from these HEK293T cells with anti-Myc and detection of FLAG-tagged SH3 in the anti-Myc immunoprecipitates show that the DLG5 SH3 domain indeed binds to the DLG5 GUK domain (Fig. 8*B*). Importantly, the binding of the DLG5^{L1642P} SH3 domain to the DLG5 GUK domain is greatly reduced. Quantification of coimmunoprecipitated SH3 domain normalized to input levels shows an ~75% reduction in the amount of coimmunoprecipitated L1642P SH3 domain (Fig. 8*C*), indicating that the L1642P mutation disrupts protein–protein interactions between DLG5 SH3 and GUK domains.

Neuronal subcellular localization of β-catenin and cell surface localization of *N*-cadherin are compromised in *Dlg5*$^{LP/LP}$ mice

How might disruption of DLG5 protein domain interactions affect dendritic spine formation and synaptogenesis? Previous work shows that DLG5 binds to β-catenin and is required for the delivery of catenin–cadherin complexes to the plasma membrane of epithelial cells and for their stabilization (Nechiporuk et al., 2007). Catenin–cadherin protein complexes are essential components of adherens junctions and synapses (Arikkath and Reichardt, 2008). β-Catenin is driven into dendritic spines upon depolarization (Murase et al., 2002) and is required for regulating synaptic strength and spine morphology in hippocampal neurons *in vitro* (Okuda et al., 2007). *N*-cadherin regulates dendritic spine density (Saglietti et al., 2007), morphology (Togashi et al., 2002), and stabilization after LTP *in vitro* in hippocampal slice cultures (Bozdagi et al., 2010; Mendez et al., 2010). The molecular mechanisms that regulate catenin–cadherin protein localization in neurons, however, are poorly understood.

To investigate whether DLG5 binds to β-catenin in the early postnatal brain, lysates from P12 *Dlg5*$^{+/+}$ and *Dlg5*$^{LP/LP}$ mouse brains were coimmunoprecipitated with anti-β-catenin antibody and immunoblotted for DLG5. We found that similar levels of DLG5 were coimmunoprecipitated with β-catenin in *Dlg5*$^{+/+}$ and *Dlg5*$^{LP/LP}$ brain lysates (Fig. 8*D*,*E*), showing that DLG5 interacts with β-catenin during early postnatal neural development and that this interaction is not directly affected by the L1642P mutation. We next examined the effect of the *Dlg5*^{LP} mutation on β-catenin, *N*-cadherin, and PSD95 protein levels and subcellular localization in cortical neurons. We performed Western blot analysis of forebrain lysates derived from P21 *Dlg5*$^{+/+}$ and *Dlg5*$^{LP/LP}$ mice and observed no significant difference in β-catenin, *N*-cadherin, or PSD95 total protein levels (Fig. 8*F*,*G*). Therefore, the effect of DLG5 on excitatory synaptogenesis and synaptic transmission is likely not due to an alteration of β-catenin or *N*-cadherin total protein levels or to a secondary effect on protein levels of other MAGUK proteins such as PSD95.

To address the effect of the *Dlg5* mutation on neuronal β-catenin localization, we cultured cortical neurons from E13.5 *Dlg5*$^{+/+}$ and *Dlg5*$^{LP/LP}$ mice for 21 DIV and then immunostained for β-catenin and vGlut1. β-catenin and vGlut1 double-positive puncta indicate synaptic β-catenin, and we observed punctate distribution of β-catenin along the dendrites of both *Dlg5*$^{+/+}$ and *Dlg5*$^{LP/LP}$ neurons; however, we found an ~30% reduction in the number of β-catenin/vGlut1 double-positive puncta in *Dlg5*$^{LP/LP}$ dendrites (Fig. 8*H*,*I*). Therefore, loss of DLG5 affects the targeting or stabilization of β-catenin in synpases of cortical neurons. These results strongly suggest that mislocalization of β-catenin contributes to the dendritic spine and synaptogenesis defects that we observed in *Dlg5*$^{LP/LP}$ neurons.

Because the *Dlg5*$^{LP/LP}$ mutation affects β-catenin localization to synapses, this interaction could serve to direct the surface localization of *N*-cadherin in cortical neurons. We used a surface biotinylation assay to assess *N*-cadherin cell surface levels in cultured cortical neurons. Although the total amount of *N*-cadherin protein remains unchanged in *Dlg5*$^{LP/LP}$ neurons compared with wild-type neurons, we observed a dramatic decrease in cell surface levels of *N*-cadherin (Fig. 8*J*). Quantification of surface *N*-cadherin levels normalized to total *N*-cadherin revealed an ~80% decrease in the fraction of *N*-cadherin targeted to the cell surface in *Dlg5*$^{LP/LP}$ neurons (Fig. 8*K*). Therefore, the DLG5^{L1642P} mutation markedly disrupts synaptic localization of β-catenin and leads to greatly decreased *N*-cadherin levels at the cortical neuronal surface.

DLG5 and *N*-cadherin interact functionally *in vitro* and *in vivo*

We found that DLG5 is required for dendritic spine formation and cell surface localization of *N*-cadherin. Previous studies on the role of *N*-cadherin in spine development and synaptic function were performed *in vitro* using hippocampal neurons (Togashi et al., 2002; Saglietti et al., 2007; Bozdagi et al., 2010; Mendez et al., 2010). In contrast, little is known about how *N*-cadherin affects these developmental processes in cortical neurons. To address this issue, we used a previously characterized shRNA (Saglietti et al., 2007) to knockdown *N*-cadherin in cortical neurons *in vitro*. Cultured cortical neurons were transfected with *N*-cadherin shRNA at DIV 8 and cultured for a total of 21 DIV. We observed a 45% decrease in dendritic spine density after *N*-cadherin knockdown (Fig. 9*A*–*D*), demonstrating that

←

(*Figure legend continued.*) density by TEM (*Dlg5*$^{+/+}$: 11.719 ± 0.534 synapses/μm^2; *Dlg5*$^{LP/LP}$: 8.75 ± 1.048 synapses/μm^2). Number of synapses quantified: $n = 75$ from 3 brains for *Dlg5*$^{+/+}$ and $n = 56$ from 3 brains for *Dlg5*$^{LP/LP}$. Error bar represents SEM. *$p < 0.05$ by two-tailed Student's *t* test. ***F***, Quantification of mean dendritic spine area by TEM (*Dlg5*$^{+/+}$: 73699.39 ± 891.08 nm^2; *Dlg5*$^{LP/LP}$: 84903.79 ± 685.4.25 nm^2). Number of spines quantified: $n = 47$ from 3 brains for *Dlg5*$^{+/+}$, and $n = 62$ from 3 brains for *Dlg5*$^{LP/LP}$. Error bar represents SEM. N.S. $p = 0.17$ by two-tailed Student's *t* test. ***G***, Quantification of mean PSD length by TEM (*Dlg5*$^{+/+}$: 201.14 ± 10.27 nm; *Dlg5*$^{LP/LP}$: 211.35 ± 8.34 nm). Number of synapses quantified: $n = 42$ from 3 brains for *Dlg5*$^{+/+}$, and $n = 67$ from 3 brains for *Dlg5*$^{LP/LP}$. Error bar represents SEM. N.S. $p = 0.7$ by two-tailed Student's *t* test. ***H***, Quantification of mean number of presynaptic vesicles by TEM (*Dlg5*$^{+/+}$: 20.1 ± 2.26; *Dlg5*$^{LP/LP}$: 24.26 ± 3.4). Number of synapses quantified: $n = 30$ from 3 brains for *Dlg5*$^{+/+}$, and $n = 34$ from 3 brains for *Dlg5*$^{LP/LP}$. Error bar represents SEM. N.S. $p = 0.36$ by two-tailed Student's *t* test. ***I***, Quantification of synaptic vesicle diameter by TEM (*Dlg5*$^{+/+}$: 22.75 ± 0.382 μm; *Dlg5*$^{LP/LP}$: 22.16 ± 0.316 μm). Number of vesicles quantified: $n = 108$ vesicles from 26 synapses from 3 brains for *Dlg5*$^{+/+}$, and $n = 134$ vesicles from 35 synapses from 3 brains for *Dlg5*$^{LP/LP}$. Scale bars: 500 nm for ***A*** and ***B***, 50 nm for ***C*** and ***D***.

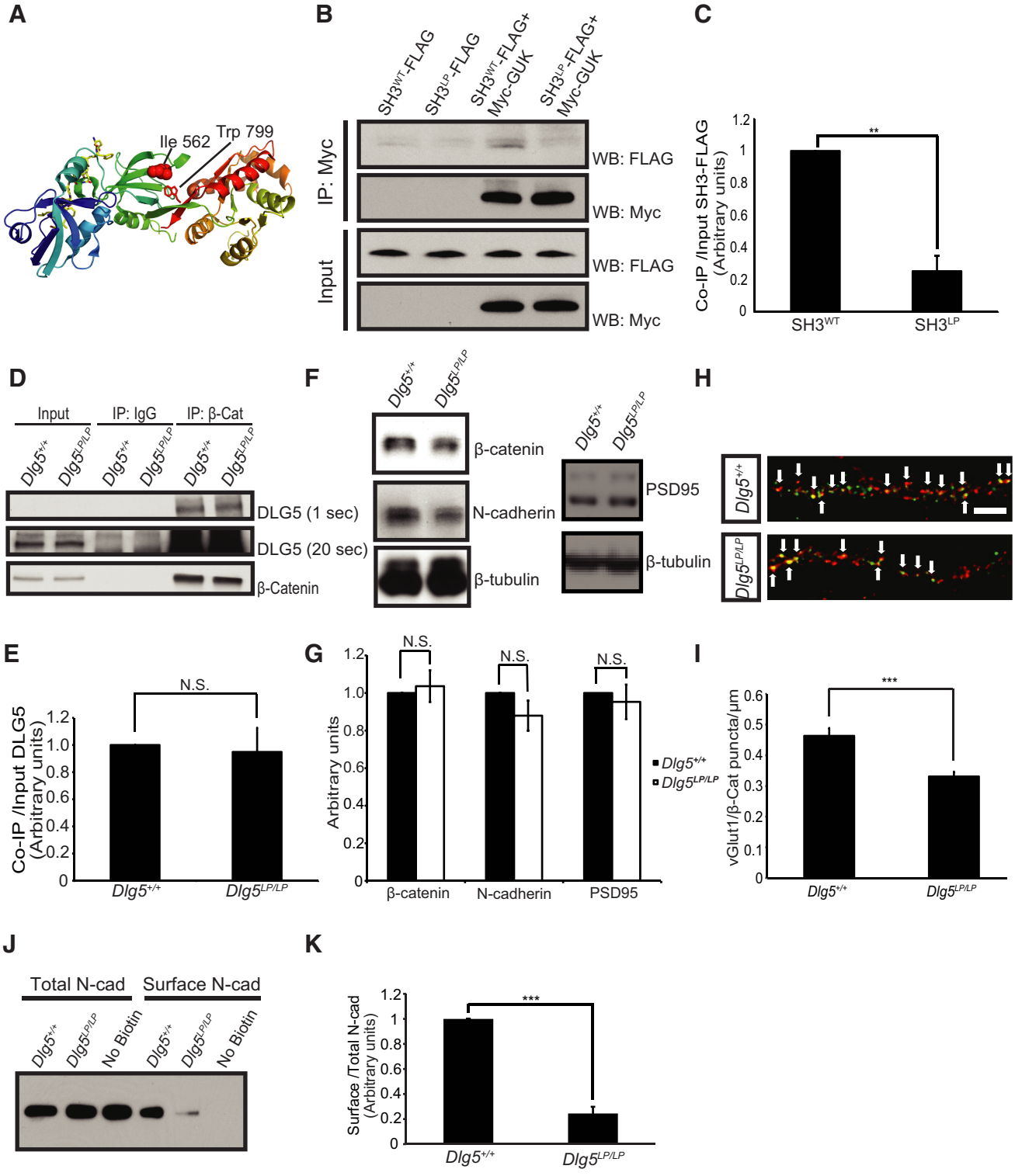

Figure 8. DLG5 regulates neuronal β-catenin and *N*-cadherin localization. ***A***, Crystal structure of human ZO-1 SH3-GUK domain presented as ribbon diagram (Nomme et al., 2011). Isoleucine 562 homologous to DLG5 leucine 1642 and tryptophan 799 are highlighted. ***B***, HEK 293T cells were transfected with FLAG-tagged wild-type SH3 alone, FLAG-tagged SH3 ^{L1642P} alone, FLAG-tagged wild-type SH3 with Myc-tagged GUK, or FLAG-tagged SH3 ^{L1642P} with Myc-tagged GUK. Cell lysates were immunoprecipitated with Myc antibody and immunoblotted for FLAG and Myc. The amount of SH3 ^{L1642P} that coimmunoprecipitated with GUK was significantly reduced compared with that of wild-type SH3. The input is 1% of the lysate used for immunoprecipitation. ***C***, Quantification shows decreased coimmunoprecipitated SH3 ^{L1642P} normalized to input levels (SH3 ^{LP}: 0.25 ± 0.095). The amount of coimmunoprecipitated SH3 ^{WT} normalized to input levels is designated as 1. Error bar represents SEM. $n = 4$ independent experiments. $^{**}p < 0.01$ by two-tailed Student's *t* test. ***D***, Brain lysates from P12 *Dlg5* $^{+/+}$ and *Dlg5* $^{LP/LP}$ mice were immunoprecipitated with β-catenin antibody and immunoblotted for β-catenin and DLG5. The input is 5% of the lysate used for immunoprecipitation. ***E***, Quantification shows similar amount of coimmunoprecipitated DLG5 normalized to input levels in *Dlg5* $^{+/+}$ and *Dlg5* $^{LP/LP}$ brain lysate (*Dlg5* $^{LP/LP}$: 0.95 ± 0.178). The amount of coimmunoprecipitated DLG5 normalized to input levels in *Dlg5* $^{+/+}$ is designated as 1. Error bar represents SEM. $n = 3$ brains for *Dlg5* $^{+/+}$ and $n = 5$ brains for *Dlg5* $^{LP/LP}$. N.S. $p = 0.801$ by two-tailed Student's *t* test. ***F***, Western-blot analysis of β-catenin, *N*-cadherin, and PSD95 protein levels in total brain lysates prepared from P21 *Dlg5* $^{+/+}$ and *Dlg5* $^{LP/LP}$ littermates. There is no significant difference in β-catenin, *N*-cadherin, and PSD95 protein levels. ***G***, Quantification of β-catenin, *N*-cadherin, and PSD95 protein levels from total brain lysates prepared from *Dlg5* $^{+/+}$ and *Dlg5* $^{LP/LP}$ littermates, normalized to *Dlg5* $^{+/+}$ protein levels (*Figure legend continues.*)

N-cadherin is also required for spine formation in cortical neurons.

If this decrease in spine density in *Dlg5*$^{LP/LP}$ neurons is indeed caused by reduction of cell surface *N*-cadherin, then this phenotype should be suppressed by *N*-cadherin gain of function. Cortical neurons cultured from E13.5 *Dlg5*$^{+/+}$ and *Dlg5*$^{LP/LP}$ mice were transfected with a construct expressing GFP-tagged *N*-cadherin at 8 DIV and then cultured for a total of 21 DIV. Although overexpression of *N*-cadherin had no effect on spine density in *Dlg5*$^{+/+}$ neurons, it restored spine density in *Dgl5*$^{LP/LP}$ neurons to wild-type levels (Fig. 9*E–H*). These results demonstrate that the reduction in spine density in *Dlg5*$^{LP/LP}$ neurons can be ameliorated by *N*-cadherin gain-of-function through overexpression.

Finally, we investigated whether *Dlg5* and *N-cadherin* genetically interact *in vivo* by performing transheterozygous genetic analysis. To obtain *N-cad*$^{+/-}$ mice, we first bred *N-cad*$^{flox/flox}$ mice (Kostetskii et al., 2005) to *Sox2-Cre* mice, inducing germline deletion of *N-cad*. *N-cad*$^{+/-}$ mice were bred to *Dlg5*$^{LP/+}$ mice to obtain *Dlg5*$^{LP/+}$*; N-cad*$^{+/-}$ mice. Layer V cortical pyramidal neurons in P21 mice were then examined using Golgi labeling. Although dendritic spine density of *Dlg5*$^{LP/+}$ or *N-cad*$^{+/-}$ cortical pyramidal neurons did not differ from wild-type, there was an ~20% reduction in spine density in *Dlg5*$^{LP/+}$*;N-cad*$^{+/-}$ *trans*-heterozygous neurons (Fig. 9*I–M*). Together, these results strongly suggest that a decrease in cell-surface *N*-cadherin is the underlying cause of the spine density reduction observed in *Dlg5*$^{LP/LP}$ neurons.

Discussion

DLG5 regulates dendritic spine development

We show here that the DLG5 MAGUK protein is an important regulator of dendritic spine and excitatory synapse density and function in cortical pyramidal neurons. Loss of DLG5 leads to a decrease in the number of dendritic spines, loss of excitatory synapses, and impaired excitatory transmission. At the molecular level, DLG5 is required for the proper localization of *N*-cadherin to the cell surface of cortical neurons. These findings describe a unique mechanism by which a MAGUK protein affects dendritic spine formation and synaptogenesis: regulating the subcellular localization of a *trans*-synaptic cell adhesion molecule.

The DLG family of MAGUK proteins includes intracellular scaffolding components composed of multiple protein interaction domains that facilitate the assembly of large molecular complexes at synapses. One of the best-studied DLG family members, PSD95, controls the localization and trafficking of glutamate receptors through direct interactions with NMDA receptors and also indirect interactions with AMPA receptors that are mediated by transmembrane AMPA receptor regulatory proteins (TARPs; Kim and Sheng, 2004). PSD95 also interacts with a myriad of signaling proteins to regulate synaptic properties and plasticity (Kim and Sheng, 2004; Feng and Zhang, 2009). Consistent with a role in regulating glutamate receptor trafficking and synaptic plasticity, PSD95 mutant mice show facilitated LTP induction, impaired LTD, and impaired spatial learning (Migaud et al., 1998; Elias et al., 2006; Cuthbert et al., 2007; Carlisle et al., 2008). In contrast, the role of PSD95 in regulating dendritic spine and synapse densities *in vivo* remains enigmatic (Migaud et al., 1998; El-Husseini et al., 2000; Béïque et al., 2006; Vickers et al., 2006). A previous study on *PSD95* mutant mice revealed an increase in spine density localized to specific dendritic segments of hippocampal neurons (Vickers et al., 2006). However, this is in contrast to earlier work showing an increase in spine density in cultured hippocampal neurons that overexpress PSD95 (El-Husseini et al., 2000). It is also not clear whether other members of the DLG family, including PSD93, SAP97, and SAP102, regulate spine formation or synaptogenesis *in vivo*. DLG5 is unique among DLG family members because of its large N terminus with additional protein domains, and it belongs to a distinct branch of the MAGUK protein family. These additional protein domains mediate DLG5 interaction with β-catenin and regulate the subcellular localization of *N*-cadherin, which is important for determining cell polarity in epithelial cells (Nechiporuk et al., 2007) and, as we show here, synaptogenesis in neurons.

N-cadherin regulation of dendritic spine formation

Previous studies in cultured hippocampal neurons identified β-catenin and *N*-cadherin as important regulators of spine morphogenesis and synaptogenesis (Togashi et al., 2002; Okuda et al., 2007; Saglietti et al., 2007). The molecular pathways that regulate *N*-cadherin subcellular localization in other developmental processes have begun to be elucidated. For example, Rab-dependent endocytic pathways regulate *N*-cadherin trafficking during cortical neuronal migration (Kawauchi et al., 2010). However, the mechanism by which *N*-cadherin is localized to dendritic spines and promotes spine formation is poorly understood. In hippocampal neurons, afadin, a Ras/Rap effector, promotes *N*-cadherin recruitment to dendritic spines (Beaudoin et al., 2012). Here, we identify DLG5 as a critical molecule for promoting cell surface localization of *N*-cadherin in cortical neurons. Although we cannot formally exclude the possibility that DLG5 regulates dendritic spine formation through other molecular interactions, suppression of the spine deficit in *Dlg5*$^{LP/LP}$ neurons by *N*-cadherin overexpression, coupled with genetic interactions between *DLG5*^{LP} and *N-cad*^{null} *in vivo*, strongly suggest that *N*-cadherin is a key effector of DLG5 function in dendritic spine formation. In contrast to previous studies in which *N*-cadherin function perturbed by overexpressing an extracellular domain-deleted *N*-cadherin resulted in altered dendritic spine morphology in cultured hippocampal neurons (Togashi et al., 2002), we did not observe a significant alteration in *Dlg5*$^{LP/LP}$ mutant cortical neuron dendritic spine morphology *in vivo*. This discrepancy may result from differences in the methods used to perturb neuronal *N*-cadherin function and/or differences between cortical and hippocampal neurons. A key early event in the elaboration of dendritic spines and synaptogenesis is the stabilization of

←

(*Figure legend continued.*) (*Dlg5*$^{LP/LP}$ β-catenin: 1.04 ± 0.084, *N*-cadherin: 0.88 ± 0.081, PSD95: 0.95 ± 0.092). $n = 5$ brains for *Dlg5*$^{+/+}$ and $n = 5$ brains for *Dlg5*$^{LP/LP}$. Error bars indicate SEM. N.S. $p = 0.690$ (β-catenin), $p = 0.171$ (*N*-cadherin), and p-0.635 by two-tailed Student's *t* test. ***H***, Cortical neurons derived from E13.5 *Dlg5*$^{+/+}$ and *Dlg5*$^{LP/LP}$ embryos were cultured for 21 DIV and stained for β-catenin and vGlut1. *Dlg5*$^{LP/LP}$ neurons show a decrease in dendritic vGlut1/β-catenin double-positive puncta (white arrows) density. ***I***, Quantification of vGlut1/β-catenin double-positive puncta density in dendrites of cortical neurons cultured for 21 DIV (*Dlg5*$^{+/+}$: 0.46 ± 0.026 puncta/μm; *Dlg5*$^{LP/LP}$: 0.33 ± 0.016 puncta/μm). Number of neurons quantified: $n = 27$ from 3 independent cultures for *Dlg5*$^{+/+}$, and $n = 27$ from 3 independent cultures for *Dlg5*$^{LP/LP}$. Error bar represents SEM. ***$p < 0.001$ by two-tailed Student's *t* test. ***J***, Cortical neurons from E13.5 *Dlg5*$^{+/+}$ *and Dlg5*$^{LP/LP}$ embryos were cultured for 21 DIV. Surface proteins were biotinylated and precipitated using streptavidin beads. The precipitate and the input (5% of the lysate used for immunoprecipitation), was immunoblotted for *N*-cadherin to reveal surface *N*-cadherin and total *N*-cadherin, respectively. Surface *N*-cadherin was decreased in *Dlg5*$^{LP/LP}$ neurons, whereas total *N*-cadherin remains the same. ***K***, Quantification of surface *N*-cadherin levels normalized to total *N*-cadherin levels (*Dlg5*$^{LP/LP}$: 0.24 ± 0.053). Cell surface *N*-cadherin normalized to total *N*-cadherin in *Dlg5*$^{+/+}$ neurons is designated as 1. Error bar represents SEM. $n = 5$ independent cultures for *Dlg5*$^{+/+}$, and 5 independent cultures for *Dlg5*$^{LP/LP}$. ***$p < 0.001$ by two-tailed Student's *t* test. Scale bar in ***D***, 10 μm.

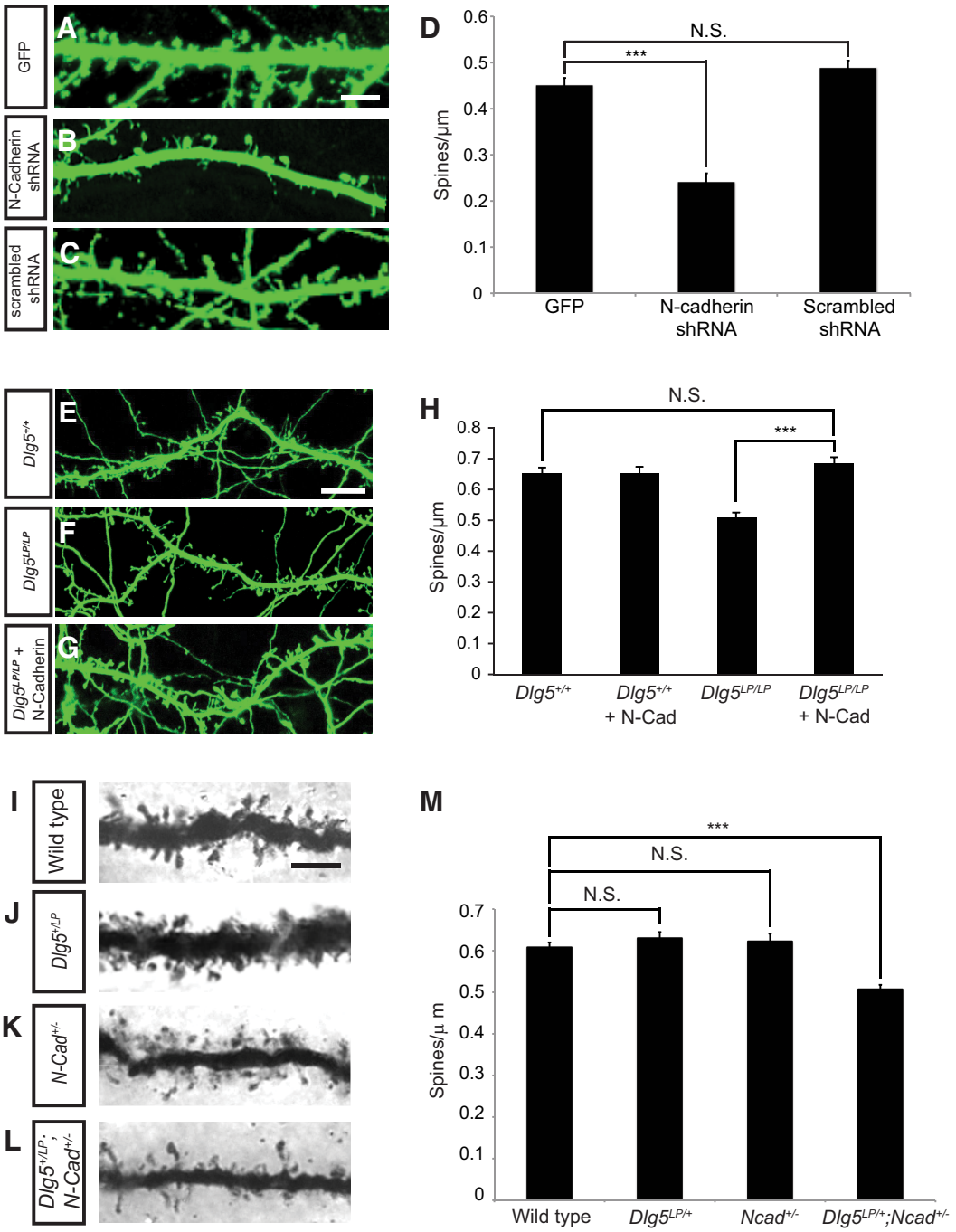

Figure 9. DLG5 regulation of dendritic spine development requires *N*-cadherin. ***A*–*C***, Cortical neurons derived from E13.5 WT embryos were transfected with constructs expressing GFP (***A***), *N*-cadherin shRNA and GFP (***B***), or scrambled shRNA and GFP (***C***) at 8 DIV and cultured for a total of 21 DIV. *N*-cadherin knockdown causes a significant decrease in dendritic spine density, whereas scrambled shRNA has no effect. ***D***, Quantification of dendritic spine density in cortical neurons at 21 DIV (GFP: 0.451 ± 0.016 spines/μm; *N*-cadherin shRNA: 0.241 ± 0.019 spines/μm; scrambled shRNA: 0.488 ± 0.016 spines/μm). Number of neurons quantified: $n = 24$ for GFP from 3 independent cultures, $n = 24$ for *N*-cadherin shRNA from 3 independent cultures, and $n = 10$ for scrambled shRNA from 3 independent cultures. Error bar represents SEM. ***$p < 0.001$ by two-tailed Student's *t* test. ***E*–*G***, Cortical neurons from E13.5 $Dlg5^{+/+}$ and $Dlg5^{LP/LP}$ embryos were transfected with constructs expressing GFP or GFP–*N*-cadherin at 8DIV and then cultured for a total of 21DIV. *N*-cadherin overexpression rescues the dendritic spine density defect in $Dlg5^{LP/LP}$ neurons. ***H***, Quantification of dendritic spine density in cultured cortical neurons at 21 DIV. ($Dlg5^{+/+}$: 0.653 ± 0.018 spines/μm; $Dlg5^{+/+}$ + *N*-cadherin: 0.653 ± 0.021 spines/μm; $Dlg5^{LP/LP}$: 0.509 ± 0.015 spines/μm; $Dlg5^{LP/LP}$ + *N*-cadhrin: 0.684 ± 0.021 spines/μm). Number of neurons quantified: $n = 27$ from 3 independent cultures for $Dlg5^{+/+}$, $n = 27$ from 3 independent cultures for $Dlg5^{+/+}$ + *N*-cadherin, $n = 27$ from 3 independent cultures for $Dlg5^{LP/LP}$, and $n = 27$ from 3 independent cultures for $Dlg5^{LP/LP}$ + *N*-cadherin. Error bar represents SEM. ***$p <$ 0.001, N.S. $p = 0.27$ by two-tailed Student's *t* test. ***I*–*L***, Layer V pyramidal neurons from wild-type (***I***), $Dlg5^{LP/+}$ (***J***), $Ncad^{+/-}$ (***K***), and $Dlg5^{LP/+}$; $Ncad^{+/-}$ (***L***) brains were examined by Golgi staining at P28. $Dlg5^{LP/+}$;$Ncad^{+/-}$ neurons show a significant reduction in dendritic spine density, whereas $Dlg5^{LP/+}$ and $Ncad^{+/-}$ neurons have normal spine density. ***M***, Quantification of dendritic spine density in layer V pyramidal neurons. (Wild-type: 0.608 ± 0.012 spines/μm; $Dlg5^{LP/+}$: 0.63 ± 0.015 spines/μm; $Ncad^{+/-}$: 0.622 ± 0.019 spines/μm; $Dlg5^{LP/+}$; $Ncad^{+/-}$: 0.507 ± 0.011 spines/μm). The number of neurons quantified: $n = 30$ neurons from 3 brains for wild-type, $n = 30$ neurons from 3 brains for $Dlg5^{LP/+}$, $n = 30$ neurons from 3 brains for $Ncad^{+/-}$, and $n = 30$ neurons from 4 brains for $Dlg5^{LP/+}$; $Ncad^{+/-}$. Error bars indicate SEM. ***$p < 0.001$ by two-tailed Student's *t* test. Scale bars: 5 μm for ***A*–*C***, 10 μm for ***E*–*G***, and 5 μm for ***I*–*L***.

trans-synaptic contacts mediated by cell surface proteins. The availability of cell adhesion molecules at the neuronal cell-surface could therefore determine whether *trans*-synaptic contacts successfully develop into synapses. In addition to providing *trans*-synaptic adhesion, *N*-cadherin may also regulate cytoskeletal dynamics in dendritic spines through multiple signaling pathways, including signaling by the Rho family of GTPases and PI3 kinase (Arikkath and Reichardt, 2008; Stepniak et al., 2009). Future work will determine whether these, or other, signaling pathways are affected by loss of DLG5.

In addition to β-catenin, DLG5 has been shown to interact with syntaxin-4 (Nechiporuk et al., 2007). Syntaxin-4 is a postsynaptic t-SNARE (target-Soluble NSF-Attachment Protein Receptor) that is involved in the exocytosis of AMPA-receptor-containing vesicles at the postsynaptic membrane during elevated synaptic activity (Kennedy et al., 2010). Future work will determine whether DLG5 promotes surface localization of catenin-cadherin complexes during synaptogenesis through interactions with syntaxin-4.

Role of the DLG5 SH3 domain in neurons

Using a forward genetic screen, we have isolated a novel *Dlg5* allele, $Dlg5^{LP}$, that harbors an L1642P substitution in the DLG5 SH3 domain. This single amino acid substitution in the DLG5 SH3 domain disrupts DLG5 protein functions required for dendritic spine formation both *in vitro* and *in vivo*. The severity of the hydrocephalus and dendritic spine deficits in the $Dlg5^{LP}$ point mutant is comparable to that of the null allele despite the presence of $DLG5^{LP}$ protein at ~50% of wild-type protein levels, demonstrating the critical role of the SH3 domain in normal DLG5 function. In invertebrates, mutations in the SH3 domain of *Drosophila* Dlg affect septate junction formation and result in lethality (Woods et al., 1996). Here, we provide *in vivo* evidence for the critical role played by the Dlg5 SH3 domain in the neuronal function of MAGUK proteins in vertebrates. Previous work on PSD95 indicates that the SH3 domain in MAGUK proteins lacks the characteristic secondary structure required for binding to proline-rich motifs (McGee et al., 2001). Instead, the PSD95 SH3 domain binds to its own GUK domain. It has been proposed that SH3-GUK domain interaction is critical for the formation of PSD95 oligomers that in turn cluster and stabilize channels, cell-adhesion molecules, and other cell surface proteins (McGee and Bredt, 1999; Colledge et al., 2000; Shin et al., 2000; Tavares et al., 2001; Kim and Sheng, 2004; Bhattacharyya et al., 2009). We show here that the *Dlg5L1642P* mutation greatly attenuates interaction between the DLG5 SH3 and GUK domains. We propose that loss of protein domain interactions critical for normal DLG5 function, together with a decrease in protein levels, leads to the decrease in synaptic β-catenin and also cell surface localization of *N*-cadherin observed in $Dlg5^{LP/LP}$ mice.

Together, our observations demonstrate that DLG5 is important for dendritic spine formation and synaptogenesis in cortical neurons. On a molecular level, DLG5 regulates synaptogenesis by controlling the subcellular localization of β-catenin and *N*-cadherin. These observations underscore the importance of MAGUK proteins in dendritic spine formation and define a molecular mechanism that mediates *N*-cadherin cell surface localization during synaptogenesis. The availability of cell adhesion molecules such as *N*-cadherin at the cell surface is a crucial determinant of *trans*-synaptic contact stabilization and subsequent synapse formation. The identification here of a novel DLG5 neuronal function lends further insight into our understanding of the molecular mechanisms that orchestrate the establishment of neural connectivity.

References

Arikkath J, Reichardt LF (2008) Cadherins and catenins at synapses: roles in synaptogenesis and synaptic plasticity. Trends Neurosci 31:487–494. CrossRef Medline

Ballesteros-Yáñez I, Benavides-Piccione R, Elston GN, Yuste R, DeFelipe J (2006) Density and morphology of dendritic spines in mouse neocortex. Neuroscience 138:403–409. CrossRef Medline

Beaudoin GM 3rd, Schofield CM, Nuwal T, Zang K, Ullian EM, Huang B, Reichardt LF (2012) Afadin, a Ras/Rap effector that controls cadherin function, promotes spine and excitatory synapse density in the hippocampus. J Neurosci 32:99–110. CrossRef Medline

Béïque JC, Lin DT, Kang MG, Aizawa H, Takamiya K, Huganir RL (2006) Synapse-specific regulation of AMPA receptor function by PSD-95. Proc Natl Acad Sci U S A 103:19535–19540. CrossRef Medline

Bhattacharyya S, Biou V, Xu W, Schlüter O, Malenka RC (2009) A critical role for PSD-95/AKAP interactions in endocytosis of synaptic AMPA receptors. Nat Neurosci 12:172–181. CrossRef Medline

Bhatt DH, Zhang S, Gan WB (2009) Dendritic spine dynamics. Annu Rev Physiol 71:261–282. CrossRef Medline

Bozdagi O, Wang XB, Nikitczuk JS, Anderson TR, Bloss EB, Radice GL, Zhou Q, Benson DL, Huntley GW (2010) Persistence of coordinated long-term potentiation and dendritic spine enlargement at mature hippocampal CA1 synapses requires N-cadherin. J Neurosci 30:9984–9989. CrossRef Medline

Carlisle HJ, Fink AE, Grant SG, O'Dell TJ (2008) Opposing effects of PSD-93 and PSD-95 on long-term potentiation and spike timing-dependent plasticity. J Physiol 586:5885–5900. CrossRef Medline

Colledge M, Dean RA, Scott GK, Langeberg LK, Huganir RL, Scott JD (2000) Targeting of PKA to glutamate receptors through a MAGUK-AKAP complex. Neuron 27:107–119. CrossRef Medline

Craig AM, Kang Y (2007) Neurexin-neuroligin signaling in synapse development. Curr Opin Neurobiol 17:43–52. CrossRef Medline

Cuthbert PC, Stanford LE, Coba MP, Ainge JA, Fink AE, Opazo P, Delgado JY, Komiyama NH, O'Dell TJ, Grant SG (2007) Synapse-associated protein 102/dlgh3 couples the NMDA receptor to specific plasticity pathways and learning strategies. J Neurosci 27:2673–2682. CrossRef Medline

de Mendoza A, Suga H, Ruiz-Trillo I (2010) Evolution of the MAGUK protein gene family in premetazoan lineages. BMC Evol Biol 10:93. CrossRef Medline

de Wit J, Sylwestrak E, O'Sullivan ML, Otto S, Tiglio K, Savas JN, Yates JR 3rd, Comoletti D, Taylor P, Ghosh A (2009) LRRTM2 interacts with Neurexin1 and regulates excitatory synapse formation. Neuron 64:799–806. CrossRef Medline

El-Husseini AE, Schnell E, Chetkovich DM, Nicoll RA, Bredt DS (2000) PSD-95 involvement in maturation of excitatory synapses. Science 290:1364–1368. Medline

Elias GM, Funke L, Stein V, Grant SG, Bredt DS, Nicoll RA (2006) Synapse-specific and developmentally regulated targeting of AMPA receptors by a family of MAGUK scaffolding proteins. Neuron 52:307–320. CrossRef Medline

Elston GN, DeFelipe J (2002) Spine distribution in cortical pyramidal cells: a common organizational principle across species. Prog Brain Res 136:109–133. CrossRef Medline

Feng W, Zhang M (2009) Organization and dynamics of PDZ-domain-related supramodules in the postsynaptic density. Nat Rev Neurosci 10:87–99. CrossRef Medline

Hayashi Y, Majewska AK (2005) Dendritic spine geometry: functional implication and regulation. Neuron 46:529–532. CrossRef Medline

Henkemeyer M, Itkis OS, Ngo M, Hickmott PW, Ethell IM (2003) Multiple EphB receptor tyrosine kinases shape dendritic spines in the hippocampus. J Cell Biol 163:1313–1326. CrossRef Medline

Irwin SA, Galvez R, Greenough WT (2000) Dendritic spine structural anomalies in fragile-X mental retardation syndrome. Cereb Cortex 10:1038–1044. CrossRef Medline

Kaufmann WE, Moser HW (2000) Dendritic anomalies in disorders associated with mental retardation. Cereb Cortex 10:981–991. CrossRef Medline

Kawauchi T, Sekine K, Shikanai M, Chihama K, Tomita K, Kubo K, Nakajima K, Nabeshima Y, Hoshino M (2010) Rab GTPases-dependent endocytic

pathways regulate neuronal migration and maturation through N-cadherin trafficking. Neuron 67:588–602. CrossRef Medline

Kayser MS, Nolt MJ, Dalva MB (2008) EphB receptors couple dendritic filopodia motility to synapse formation. Neuron 59:56–69. CrossRef Medline

Kennedy MJ, Davison IG, Robinson CG, Ehlers MD (2010) Syntaxin-4 defines a domain for activity-dependent exocytosis in dendritic spines. Cell 141:524–535. CrossRef Medline

Kim E, Sheng M (2004) PDZ domain proteins of synapses. Nat Rev Neurosci 5:771–781. CrossRef Medline

Knobloch M, Mansuy IM (2008) Dendritic spine loss and synaptic alterations in Alzheimer's disease. Mol Neurobiol 37:73–82. CrossRef Medline

Ko J, Fuccillo MV, Malenka RC, Südhof TC (2009) LRRTM2 functions as a neurexin ligand in promoting excitatory synapse formation. Neuron 64: 791–798. CrossRef Medline

Kostetskii I, Li J, Xiong Y, Zhou R, Ferrari VA, Patel VV, Molkentin JD, Radice GL (2005) Induced deletion of the N-cadherin gene in the heart leads to dissolution of the intercalated disc structure. Circ Res 96:346–354. CrossRef Medline

Lippman J, Dunaevsky A (2005) Dendritic spine morphogenesis and plasticity. J Neurobiol 64:47–57. CrossRef Medline

McGee AW, Bredt DS (1999) Identification of an intramolecular interaction between the SH3 and guanylate kinase domains of PSD-95. J Biol Chem 274:17431–17436. CrossRef Medline

McGee AW, Dakoji SR, Olsen O, Bredt DS, Lim WA, Prehoda KE (2001) Structure of the SH3-guanylate kinase module from PSD-95 suggests a mechanism for regulated assembly of MAGUK scaffolding proteins. Mol Cell 8:1291–1301. CrossRef Medline

Mendez P, De Roo M, Poglia L, Klauser P, Muller D (2010) N-cadherin mediates plasticity-induced long-term spine stabilization. J Cell Biol 189: 589–600. CrossRef Medline

Merte J, Wang Q, Vander Kooi CW, Sarsfield S, Leahy DJ, Kolodkin AL, Ginty DD (2010b) A forward genetic screen in mice identifies Sema3A(K108N), which binds to neuropilin-1 but cannot signal. J Neurosci 30:5767–5775. CrossRef Medline

Merte J, Jensen D, Wright K, Sarsfield S, Wang Y, Schekman R, Ginty DD (2010a) Sec24b selectively sorts Vangl2 to regulate planar cell polarity during neural tube closure. Nat Cell Biol 12:41–46; sup pp 1–8. CrossRef Medline

Migaud M, Charlesworth P, Dempster M, Webster LC, Watabe AM, Makhinson M, He Y, Ramsay MF, Morris RG, Morrison JH, O'Dell TJ, Grant SG. (1998) Enhanced long-term potentiation and impaired learning in mice with mutant postsynaptic density-95 protein. Nature 396:433–439. CrossRef Medline

Murase S, Mosser E, Schuman EM (2002) Depolarization drives beta-Catenin into neuronal spines promoting changes in synaptic structure and function. Neuron 35:91–105. CrossRef Medline

Nechiporuk T, Fernandez TE, Vasioukhin V (2007) Failure of epithelial tube maintenance causes hydrocephalus and renal cysts in Dlg5-/- mice. Dev Cell 13:338–350. CrossRef Medline

Nimchinsky EA, Sabatini BL, Svoboda K (2002) Structure and function of dendritic spines. Annu Rev Physiol 64:313–353. CrossRef Medline

Nomme J, Fanning AS, Caffrey M, Lye MF, Anderson JM, Lavie A (2011) The Src homology 3 domain is required for junctional adhesion molecule binding to the third PDZ domain of the scaffolding protein ZO-1. J Biol Chem 286:43352–43360. CrossRef Medline

Okuda T, Yu LM, Cingolani LA, Kemler R, Goda Y (2007) beta-Catenin regulates excitatory postsynaptic strength at hippocampal synapses. Proc Natl Acad Sci U S A 104:13479–13484. CrossRef Medline

Penzes P, Cahill ME, Jones KA, VanLeeuwen JE, Woolfrey KM (2011) Dendritic spine pathology in neuropsychiatric disorders. Nat Neurosci 14: 285–293. CrossRef Medline

Saglietti L, Dequidt C, Kamieniarz K, Rousset MC, Valnegri P, Thoumine O, Beretta F, Fagni L, Choquet D, Sala C, Sheng M, Passafaro M (2007) Extracellular interactions between GluR2 and N-cadherin in spine regulation. Neuron 54:461–477. CrossRef Medline

Saneyoshi T, Fortin DA, Soderling TR (2010) Regulation of spine and synapse formation by activity-dependent intracellular signaling pathways. Curr Opin Neurobiol 20:108–115. CrossRef Medline

Shin H, Hsueh YP, Yang FC, Kim E, Sheng M (2000) An intramolecular interaction between Src homology 3 domain and guanylate kinase-like domain required for channel clustering by postsynaptic density-95/SAP90. J Neurosci 20:3580–3587. Medline

Siddiqui TJ, Craig AM (2011) Synaptic organizing complexes. Curr Opin Neurobiol 21:132–143. CrossRef Medline

Spruston N (2008) Pyramidal neurons: dendritic structure and synaptic integration. Nat Rev Neurosci 9:206–221. CrossRef Medline

Stepniak E, Radice GL, Vasioukhin V (2009) Adhesive and signaling functions of cadherins and catenins in vertebrate development. Cold Spring Harb Perspect Biol 1:a002949. CrossRef Medline

Suzuki SC, Takeichi M (2008) Cadherins in neuronal morphogenesis and function. Dev Growth Differ 50:S119–S130. CrossRef Medline

Tada T, Sheng M (2006) Molecular mechanisms of dendritic spine morphogenesis. Curr Opin Neurobiol 16:95–101. CrossRef Medline

Tavares GA, Panepucci EH, Brunger AT (2001) Structural characterization of the intramolecular interaction between the SH3 and guanylate kinase domains of PSD-95. Mol Cell 8:1313–1325. CrossRef Medline

Togashi H, Abe K, Mizoguchi A, Takaoka K, Chisaka O, Takeichi M (2002) Cadherin regulates dendritic spine morphogenesis. Neuron 35:77–89. CrossRef Medline

Tran TS, Rubio ME, Clem RL, Johnson D, Case L, Tessier-Lavigne M, Huganir RL, Ginty DD, Kolodkin AL (2009) Secreted semaphorins control spine distribution and morphogenesis in the postnatal CNS. Nature 462:1065–1069. CrossRef Medline

Vickers CA, Stephens B, Bowen J, Arbuthnott GW, Grant SG, Ingham CA (2006) Neurone specific regulation of dendritic spines in vivo by post synaptic density 95 protein (PSD-95). Brain Res 1090:89–98. CrossRef Medline

Woods DF, Hough C, Peel D, Callaini G, Bryant PJ (1996) Dlg protein is required for junction structure, cell polarity, and proliferation control in *Drosophila* epithelia. J Cell Biol 134:1469–1482. CrossRef Medline

Yagi T, Takeichi M (2000) Cadherin superfamily genes: functions, genomic organization, and neurologic diversity. Genes Dev 14:1169–1180. CrossRef Medline

Yoshihara Y, De Roo M, Muller D (2009) Dendritic spine formation and stabilization. Curr Opin Neurobiol 19:146–153. CrossRef Medline

Zhou Z, Hong EJ, Cohen S, Zhao WN, Ho HY, Schmidt L, Chen WG, Lin Y, Savner E, Griffith EC, Hu L, Steen JA, Weitz CJ, Greenberg ME. (2006) Brain-specific phosphorylation of MeCP2 regulates activity-dependent Bdnf transcription, dendritic growth, and spine maturation. Neuron 52: 255–269. CrossRef Medline